Mechanical Behavior of Unidirectional Fiber Reinforced Soft Composites

Chung-Yuen $Hui^{1,2*}$, Zezhou Liu^1 , Stuart Leigh Phoeni x^1 , Daniel R. King 2,3 ,

Wei Cui⁴, Yiwan Huang^{3,+}, and Jian Ping Gong^{2,3,5}

¹Field of Theoretical & Applied Mechanics, Deptartment of Mechanical & Aerospace Engineering, Cornell University, Ithaca, NY 14853, USA

²Global Station for Soft Matter, GI-CoRE, Hokkaido University, Sapporo 001-0021, Japan

³Faculty of Advanced Life Science, Hokkaido University, Japan

⁴Graduate School of Life Science, Hokkaido University, Japan

⁵Institute for Chemical Reaction Design and Discovery (WPI-ICReDD), Hokkaido University, Japan

⁺Current address: School of Materials and Chemical Engineering, Hubei University of Technology, China

*Corresponding Author, 322 Thurston Hall, Cornell University, Ithaca, NY 14853, USA. ch45@cornell.edu

Abstract: An upper estimate for fiber/matrix modulus ratio in traditional fiber reinforced polymer (FRP) composites is 100. Matrices made from tough elastic gels can have modulus approaching kilopascals and increase this ratio to 10⁷. We study how this extremely high modulus ratio affects the mechanical behavior of such fiber reinforced "soft" composites (FRSCs). We focus on unidirectional FRSCs with parallel fibers perfectly bonded to a soft elastic matrix. We show such composites exhibit the Mullins effect typically observed in rubbers and double network (DN) gels. We quantify size effect on mechanical properties by studying unidirectional composites consisting of *finite length* fibers. We determine the stress concentration factors (SCFs) for a cluster of fiber breaks in this geometry and show that there is a transition from equal load sharing (ELS) to local load sharing (LLS). We also determine the mean strength and work of extension assuming fibers obey Weibull statistics. We discuss the application of fracture mechanics to this emerging class of composites. We highlight similarities and differences between FRSCs and DN gels.

Keywords: Equal load sharing; Stress concentration; Mullins effect; Fiber statistics; Fracture

1. Introduction

Fiber reinforced polymer (FRP) composites are widely used in many important technological applications. For example, approximately 50% of the wings and fuselage of the Boeing 787 Dreamliner and the Airbus A350 XWB consist of carbon fiber reinforced epoxy matrix composites [1]. FRP composites have high strength to

weight ratio and are generally more resistant to fracture and damage than traditional homogenous materials. For example, failure of homogeneous solids is often preceded by the growth of a crack. In composites, failure occurs by diffuse damage due to individual fiber breaks as the composite is loaded until clusters of breaks joined together causing failure.

There is a vast literature on FRP composites. Here we focus on an emerging class of FRP composites where the matrix is extremely *soft* and tough, namely fiber reinforced soft composites (FRSCs). An early example is a composite consisting of a soft and tough alginate–polyacrylamide hydrogel reinforced with a random network of stainless steel fibers (steel wool) [2]. Feng et al. [3] use a model soft composite consisting of nylon fabric mesh adhesively bonded to VHB (very high bond) acrylic tapes to demonstrate the failure and toughening mechanism of double network (DN) gels. King et al. [4], and Huang et al. [5,6] have discovered that extremely tough composites can be made by binding a woven glass fiber fabric with a matrix consisting of a polyampholyte (PA) hydrogel [7]. These works open the possibility of making very tough composites by replacing traditional stiff epoxy matrices with soft matrices such as DN and self-healing hydrogels. The shear modulus of these soft matrices can be as low as kilopascals and they have much higher failure strain in a tension test in comparison with epoxy. For example, the PA hydrogel used by King et al. [4] after deswelling contains about 50 wt% water, has a Young's modulus of 0.1 MPa, failure strain of 30 and work of extension of 4 MJ/m³. These type of composites have many potential applications since the properties of hydrogels can be tailored to include properties such as bio-compatibility [8,9], self-healing [10,11], low friction [12] and anti-fouling [13]. For example, soft composites can be used as a robotic hand to grip and interact with a large variety of objects [14].

The FRSCs studied by King et al. [4] are made by bonding a woven glass fabric to a tough PA matrix. From a theoretical standpoint, woven fabric is a difficult system to analyze due to the large number of variables such as weave geometry, compaction, bending rigidity and friction behavior of yarns [15–17]. As noted by Scelzo et al. [15], these variables "influence in-fabric behavior such as crimp interchange, shear transfer and intervarn normal forces". The lack of a comprehensive model predicting the mechanical behavior (such as tearing strength) of fabrics motivates us to study a simpler modeling system: a unidirectional composite consisting of parallel fibers bonded to a soft elastic matrix, as shown in Fig. 1.

The analysis presented here borrows heavily from the vast literature on the mechanics of FRP composites. The readers who are unfamiliar with the mechanics of unidirectional composites may want to consult some of the excellent reviews on this topic, e.g., [18,19].

The plan of this paper is as follows: Section 2 focuses on the mechanics of unidirectional FRSCs. In this section we introduce the geometry of the composite to be studied and highlight the concept of load transfer length. We compute the stress concentration factor (SCF) on fibers next to a cluster of fiber breaks and relate this to the concept of local load sharing (LLS) [20–25] and equal load sharing (ELS) [26–28]. We also explore flaw

sensitivity. Section 3 focuses on fiber statistics and their effects on composite strength and energy dissipation. In particular, we show FRSCs exhibit the Mullins effect and use the chain-of-ELS-bundles model, which has been widely studied in the literature [18,23,27], as a model to show that the strength of FRSCs is not particularly sensitive to the composite size. We end this section with a detailed discussion of fracture mechanics approach to FRSCs. Section 4 consists of summary and discussion. In the discussion we highlight differences and similarities between DN gels and FRSCs.

2. Mechanics of unidirectional FRSCs

2.1 FRSCs have extremely high modulus ratio – large load transfer length

An important feature of FRSCs is that the fiber modulus E_f is typically five to six orders of magnitude greater than the shear modulus μ_m of the matrix. For example, most soft matrices have a shear modulus on the order of 0.1 MPa or less, whereas E_f for E-glass fiber reinforced polymer (E-GFRP) composites is on the order of 75 GPa. Thus, $E_f/\mu_m \approx 75 \times 10^9/10^5 = 7.5 \times 10^5$. Using high modulus carbon fibers where $E_f = 240$ GPa, this ratio is even higher, $E_f/\mu_m \approx 240 \times 10^9/10^5 = 2.4 \times 10^6$. To gain perspective, the same ratio for an E-glass fiber reinforced epoxy matrix composite is about $E_f/\mu_m \approx 75 \times 10^9/1.25 \times 10^9 \sim 60$, at least four orders of magnitude lower. Thus, a distinguishing feature of FRSCs is their extremely high modulus ratio.

Load transfer length

When a fiber breaks in the composite (see Fig. 1), the segments of the fiber adjacent to the break unload and the original load carried by this segment is transferred to neighboring intact fibers, causing these fibers to overload and making them more susceptible to failure. The size of this overload region is roughly the same as the length of the unloaded fiber segments and is an important length scale in composite theory [20,29]; we call this the *load transfer length* l_T . For elastic fibers and matrix and assuming perfect bonding, l_T is [20]

$$l_T = \sqrt{\frac{E_f A_f w}{\mu_m h}} \qquad , \tag{1}$$

where w is the effective width between adjacent fibers, h is the effective matrix thickness, and A_f is the cross-sectional area of a fiber (see Fig. 1). In most situations, h is roughly the main dimension of the fiber. For example, for fiber with a square cross-section, $A_f = h^2$. The spacing w is related to the volume fraction of fibers in the composite, $V_f \approx \frac{h}{h+w}$. Thus, to within a constant of order one,

$$l_T = \sqrt{\frac{E_f A_f w}{\mu_m h}} \approx \sqrt{\frac{E_f A_f}{\mu_m} \left(\frac{1}{V_f} - 1\right)}$$
 (2)

Since V_f is between 50% to 65% in most composites, the load transfer length is at least 100-1000 times the fiber diameter for FRSCs. If we take a typical fiber diameter to be 20 microns, then l_T is roughly between 2 mm to 3 cm for stiff fibers and soft matrices; this dimension is comparable to the size of samples often used for mechanical testing in a laboratory.

2.2 Stress concentration near fiber breaks: size effect

Failure of composites is controlled by stress concentration near fiber breaks. When the matrix is elastic, such models are often referred to as local load sharing (LLS) models, since the load transfer from a failed fiber tends to be concentrated on the closest unbroken fibers. The seminal work of Hedgepeth [20] provides an exact solution for the stress distribution near fiber breaks in a unidirectional fiber-matrix composite consisting of a 2D planar sheet with a parallel array of *infinitely long fibers* $(L = \infty)$ perfectly bonded to an elastic matrix, as shown in Fig. 1. Since the size of typical samples in mechanical testing are on the order of centimeters, the fibers in a composite sample with an epoxy matrix can be considered as infinitely long in comparison with the load transfer length which is typically less than 0.1 mm. This is not the case for FRSCs. This motivates us to study *size effect*, that is, instead of infinitely long fibers, the length of fibers in our unidirectional composite is *finite*. Specifically, the composite consists of a 2D array of parallel fibers of length 2L and Young's modulus E_f . The fibers are perfectly bonded to an elastic matrix of shear modulus μ_m . The composite is infinite in the x direction and has x consecutive fiber breaks (crack) along the center line y = 0. A uniform vertical displacement $\pm \Delta$ is imposed on the upper and lower surfaces of the composite plate at $y = \pm L$, thus the strain far away from the crack is $\varepsilon = \Delta/L$. All fibers have the same cross-sectional area A_f .

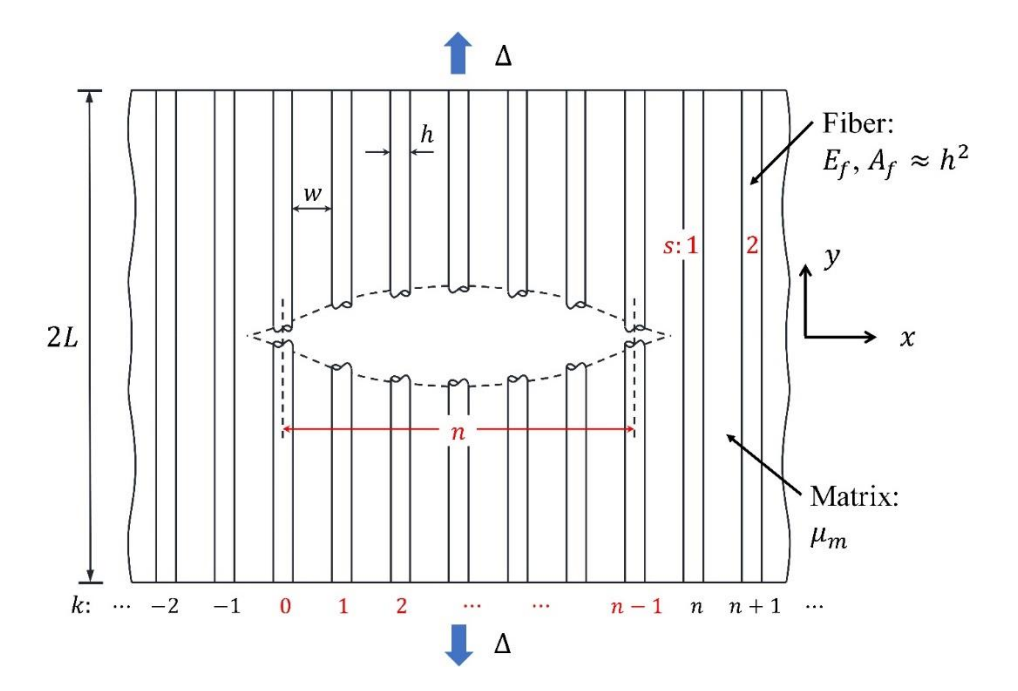


Fig. 1. Planar 2D composite with elastic fibers embedded in an elastic matrix. A group of n consecutive fibers is broken, forming a crack-like structure. The height of the composite is 2L (in Hedgepeth $L \to \infty$), and a uniform vertical displacement $\pm \Delta$ is imposed on the upper and lower surface of the composite. Integer k is used to label fibers where $-\infty < k < \infty$, and the n contiguous broken fibers (crack) span $0 \le k < n-1$. s is the number of the intact fibers ahead of the last broken fiber along the crack plane.

2.3 Flaw sensitivity

Most homogeneous material such as metals, glasses and polymers are macroscopically isotropic and *flaw* sensitive. Composites are designed to be *flaw insensitive*. This is due to the large differences in elastic modulus between the fiber and matrix. As we have already seen, the modulus ratio is roughly 100 even in traditional fiber-epoxy composites. This modulus disparity means that practically all the tension load is carried by the fibers. The only situation where matrix comes into play is near a fiber break, where it transfers the lost load of the broken fiber to other intact fibers by deforming in shear [18,20,21]. In the following, we will study the effect of composite size and modulus ratio on flaw sensitivity.

2.4 Discrete shear-lag model (DSLM) and continuum model (CM) for SCF

There are two solution methods to the stress concentration problem. The first is due to Hedgepeth [20] which we shall call the discrete shear-lag model (DSLM). Details can be found in Hedgepeth [20] and Hikami and Chou [30]. The key idea is that fibers can support only tension and the matrix can only carry shear. The fibers are discrete entities and are labeled by an integer k. For example, $u_k(y)$ and $p_k(y)$ denote the displacement and load of the k-th fiber in the 2D infinite array in Fig. 1. The governing equations for *normalized* fiber displacements is an infinite system of ordinary differential equations (ODEs) given by [20]

$$\frac{\partial^2 U_k}{\partial \xi^2} + U_{k+1} - 2U_k + U_{k-1} = 0 \qquad k = \dots, -3, -2, -1, 0, 1, 2, 3, \dots$$
(3a)

The boundary conditions of the finite fiber length problem in Fig. 1 are [31]:

$$U_k(0) = 0 \quad (k < 0, \ k \ge n), \quad \frac{dU_k}{d\xi}(0) = 0 \quad (0 \le k \le n - 1), \quad U_k(L/l_T) = L/l_T,$$
 (3b)

where

$$\xi = y/l_T, \ U_k = \frac{u_k}{\varepsilon l_T}, \ \varepsilon = \Delta/L.$$
 (3c)

Numerical solution of DSLM model can be obtained by most boundary value problem (BVP) solvers (e.g., bvp4c in Matlab, or solve bvp in Python).

Alternatively, the unidirectional composite in Fig. 1 can be modeled as a plane stress orthotropic solid [32,33] with the stresses $\sigma_{\alpha\beta}$ related to the in-plane strains $\varepsilon_{\alpha\beta}$ by

$$\sigma_{11} = C_{11}\varepsilon_{11} + C_{12}\varepsilon_{22}$$

$$\sigma_{22} = C_{12}\varepsilon_{11} + C_{22}\varepsilon_{22} ,$$

$$\sigma_{12} = 2C_{66}\varepsilon_{12}$$
(4a-c)

where the C_{ij} 's are stiffness coefficients with units of stress. For stiff fibers and soft matrices, $C_{11} \ll C_{22}$ and $C_{12} \approx C_{66} \ll C_{22}$. Using the rule of mixtures [32],

$$C_{12} \approx \frac{\mu_m}{1 - V_f}$$
, and $C_{22} \approx V_f E_f$, (4d)

provided $E_f >> \mu_m$. For the composite in Figure 1, Hui et al. [31] have shown that an excellent approximation is to neglect σ_{11} with

$$\sigma_{22} = C_{22}\varepsilon_{22} = C_{22}\partial u / \partial y \sigma_{12} = 2C_{12}\varepsilon_{12} = C_{12}\partial u / \partial x$$
(5a,b)

where u is the displacement along the fiber direction. The governing equation for the stress and deformation field u is [31–33]

$$C_{12} \frac{\partial^2 u}{\partial x^2} + C_{22} \frac{\partial^2 u}{\partial y^2} = 0.$$
 (6)

2.5 Stress concentration factor (SCF)

Linear elastic fracture mechanics (LEFM) predicts that the stress at a fiber break right next to the crack is infinite. LEFM typically assumes that the material is isotropic, homogenous and elastic all the way to the crack tip. However, fiber composites are inhomogeneous and anisotropic. As a result, continuum solutions for cracks must be interpreted carefully due to the discreteness of fiber geometry near the crack tip. Indeed, since fibers are the main load bearing agent, the relevant quantity is the stress concentration on unbroken fibers. The theory of fiber stress concentration was first established by Hedgepeth [20]. He uses the DSLM to compute the SCF for an infinite sheet of unidirectional composite loaded by remote tension σ_{∞} . His solution showed that the SCF $K_{n,1}^{L=\infty} = \sigma_1/\sigma_{\infty}$ for the first fiber right next to a single fiber break is exactly 4/3, where σ_1 is the maximum stress on the first fiber to the right of the break. The superscript 'L' in $K_{n,1}^L$ indicates that fibers have length 2L; the first subscript denotes the number of breaks (n) in the cluster and the second subscript denotes fiber s=1 ahead of the cluster. For the case of n consecutive breaks or a cluster of n breaks, the SCF on the fiber right next to the last break is found to be:

$$K_{n,1}^{\infty} = \frac{4 \cdot 6 \cdots (2n+2)}{3 \cdot 5 \cdots (2n+1)} = \frac{2^{2n} n! (n+1)!}{(2n+1)!}.$$
 (7)

Note $K_{1,1}^{\infty} = 4/3$, $K_{2,1}^{\infty} = 8/5$, $K_{3,1}^{\infty} = 64/35$, $K_{4,1}^{\infty} = 128/63$, so by the fourth fiber break the SCF on the first intact fiber has more than doubled. For very large n, the SCF approaches $\sqrt{\pi n/4}$ asymptotically [18].

Since the strength of fiber is non-deterministic, it is not always true that the highest stressed fiber fails first. It is therefore of interest to study $K_{n,s}^L$ for s > 1. The SCF $K_{n,s}^{\infty}$ was obtained by Hikami and Chou [30], i.e.

$$K_{n,s}^{\infty} = (n+2s-1)\frac{(2s)(2s+2)(2s+4)\cdots(2s+2n-2)}{(2s-1)(2s+1)(2s+3)\cdots(2s+2n-1)}.$$
(8)

Although (7) and (8) are exact, they work only for *infinitely long fibers* ($L = \infty$) and they are rather cumbersome to use. Recently, Hui et al. [31] used a continuum model (CM) based on equations (4-6) to obtain the following formula for the SCF for finite length fibers. The geometry of the CM is shown in Fig. 2. The SCF is found to be:

$$K_{n,s}^{L} = \frac{1 - \sqrt{\exp(-\pi(2s + n - 1)/\overline{L})}}{\sqrt{\left(1 - \exp\left[-\frac{\pi}{\overline{L}}\left(s - \frac{2}{3}\right)\right]\right)\left(1 - \exp\left(-\frac{\pi}{\overline{L}}\left(s + n - \frac{1}{3}\right)\right)\right)}} \qquad \overline{L} = L/l_T, \ s, n \ge 1.$$

$$(9)$$

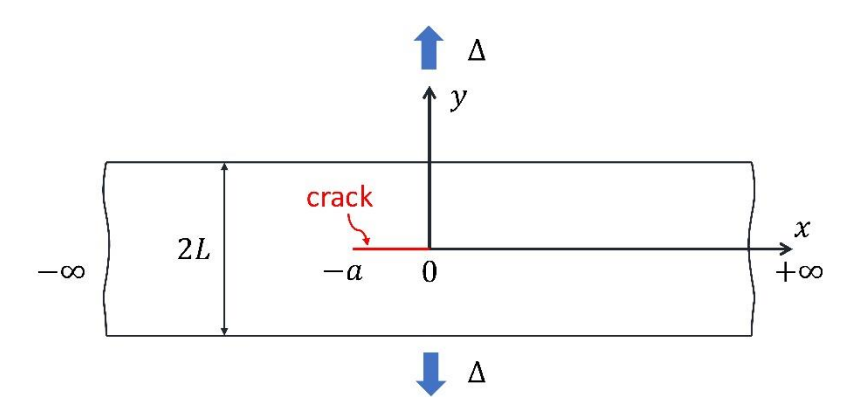


Fig. 2. Geometry of the continuum model. The fibers and matrix in Fig. 1 are homogenized and replaced by a highly anisotropic solid. The fiber breaks are modeled as a traction free crack with length *a*.

Fig. 3 compares the $K_{n,s}^L$ for n=1,2,3,4 with different normalized fiber length or composite height. The cross symbols are the analytical solution given by (9) and the circles are numerical results obtained by solving the DSLM based on (3a, b). It shows that the expression given by (9) can accurately predict the SCF for the full range of L, n and s. In the limit of a plate with infinitely long fibers where $\overline{L} = L/l_T \to \infty$, the SCF given by (9) reduces to

$$K_{n,s}^{\infty} = \frac{s + \frac{n-1}{2}}{\sqrt{\left(s - \frac{2}{3}\right)\left(s + n - \frac{1}{3}\right)}} \qquad s, n \ge 1.$$
 (10)

Equation (10) is found to be very accurate (see Fig. 3 below, for $\overline{L} = 10$) and is much easier to use than (8).

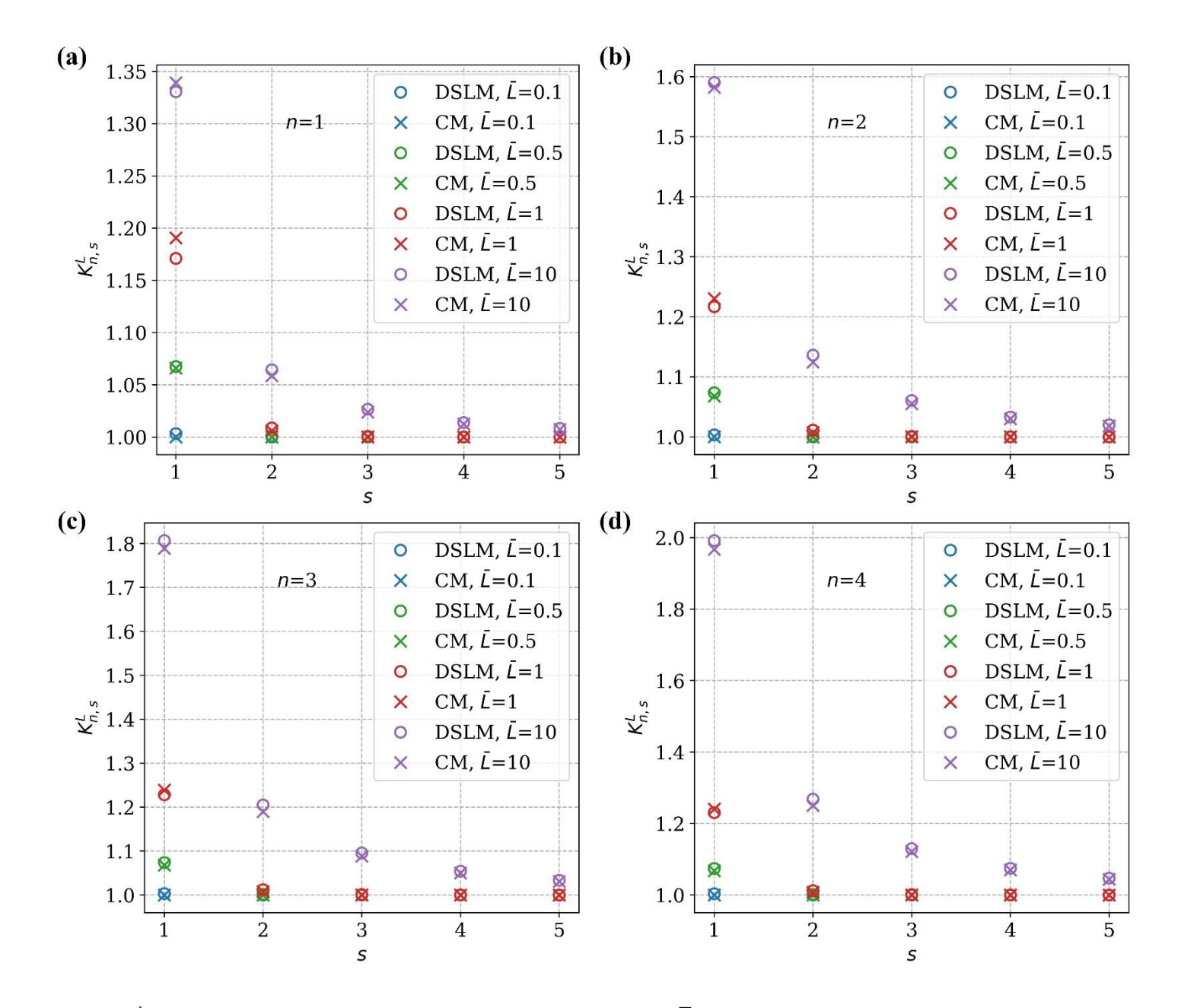


Fig. 3. $K_{n,s}^L$ in the intact fiber s with different normalized length \overline{L} . The solutions by DSLM and CM are plotted as circles and crosses, respectively. (a) n = 1; (b) n = 2; (c) n = 3; (d) n = 4.

A surprising result is that $K_{n,s}^{\infty}$ for a composite with *infinitely* long fibers and finite crack length (i.e., finite number of fiber breaks) is *independent of fiber size*, *matrix spacing and material properties*. However, this is NOT the case when fibers have finite length. Recall in FRSCs, the load transfer length l_T can be very large (centimeters), hence fiber length in a typical laboratory specimen can be less than or on the order of the load transfer length. This brings up another important result. Fig. 3 shows that for short composites, that is, if $\overline{L} < 1$, all the unbroken fibers are under ELS, that is, *all intact fibers bear the same load*, at least for n = 1,2,3,4. This result is easy to see using (9): the numerator and denominator in (9) approach 1 *exponentially fast* when $\overline{L} \to 0$.

2.6 Size effect and fracture mechanics

To persuade the above idea further, we consider the limit of an *infinitely long crack*, that is, $a \to \infty$ in Fig. 2 and Fig. 3. The SCF for this case is obtained by taking n as it approaches infinity in (9) and is:

$$K_{\infty,s}^{L} = \frac{1}{\sqrt{1 - \exp\left[-\frac{\pi}{L}\left(s - \frac{2}{3}\right)\right]}}, \quad s \ge 1.$$

$$(11)$$

In particular, when $\overline{L}=1/3$ (short composite), the exponential factor in (11) is $\exp(-\pi)$ for the first intact fiber ahead of the crack tip (s=1). For the second intact fiber s=2, this factor decreases to $\exp(-4\pi)$. Hence, in short composites, the intact fibers are practically under ELS, *irrespective of crack size*. In this regime, the composite is extremely *flaw insensitive*. Since L is on the order of centimeters for FRSCs, there is a significant range of specimen sizes where classical fracture mechanics breaks down: even *long prefabricated* cracks have no effect on fracture. To emphasize this point, the energy release rate of the infinitely long crack ($a \to \infty$) in Fig. 2 is $\left(C_{22}\varepsilon^2/2\right) \times 2L = C_{22}\varepsilon^2L$. However, for $L < l_T$, the system is under ELS, so failure of the sample is not affected by the pre-existing crack, so the use of energy release rate to characterize fracture is meaningless. As we shall see below, failure of the cracked sample in this regime is governed by random fiber breakage.

On the other hand, if L is much <u>longer</u> than the load transfer length (but still much less than the crack length), then a simple calculation using equation (9) (with $n = \infty$) shows that the stress on the first fiber directly ahead of the crack tip (s = 1) is:

$$\sigma_{22}\left(s=1\right) = C_{22}\varepsilon\sqrt{\frac{3L}{\pi l_T}} \ . \tag{12}$$

Thus, the SCF on the first fiber (s = 1) increases as the *square root of the height* of the plate, consistent with *LEFM*. In this limit, the use of fracture mechanics may be justified. We will discuss the use of fracture approach in FRSCs after we discuss fiber statistics.

3. Statistical analysis for FRSCs

3.1 Fiber statistics

If fiber strength is deterministic, that is, if all fibers in the composite break at some fixed critical stress σ_f , then once one fiber breaks, all the fibers in the composite in Fig. 1 will break irrespectively of the size of the specimen. The strength of the composite is unique and independent of size – this hypothesis is not supported by experiments. Indeed, it has been well documented that the strength of fibers is not deterministic [18,19,34,35] due to the existence of randomly occurring flaws. In particular, shorter fibers are stronger since they have less flaws. This effect is incorporated in the Weibull statistic theory of fiber strength [36]. In this theory, flaws occur

along the fiber following a compound Poisson process where the rate parameter (the average number of flaws per unit length with strength less than or equal to the stress acting on the fiber) depends on the stress acting on the fiber. Specifically, the failure probability that a fiber of length L will break when subjected to a tensile stress less than or equal to σ is

$$F(\sigma, L) = 1 - \exp \left| -\frac{L}{L_0} \left(\frac{\sigma}{\sigma_0} \right)^{\rho} \right| = 1 - \exp \left| -\left(\frac{\sigma}{\sigma_L} \right)^{\rho} \right|, \tag{13}$$

where σ_0 is the reference stress associated with a reference length L_0 , $\rho > 0$ is the Weibull shape parameter and $\sigma_L = \sigma_0 \left(L_0 / L \right)^{1/\rho}$ is the *scale parameter* for length L. In the Weibull model, the mean strength of a fiber of length L_0 is $\bar{\sigma}_0 = \sigma_0 \Gamma \left(1 + 1/\rho \right)$ (Γ is the Gamma function). For most fibers, $3 < \rho < 12$, so $0.89 \le \Gamma \left(1 + 1/\rho \right) < 0.96$. The smaller the value of ρ , the higher the variability of fiber strength. The expression $\sigma_L = \sigma_0 \left(L_0 / L \right)^{1/\rho}$ shows that the mean strength of a fiber $\bar{\sigma}_L$ changes with its length L according to

$$\bar{\sigma}_L = \left(\frac{L_0}{L}\right)^{1/\rho} \bar{\sigma}_0 \tag{14}$$

For example, decreasing the length of a fiber by a factor of 10 will increase its strength by $10^{1/\rho}$; for $\rho = 3$, the strength increases by a factor of 2.15.

3.2 Failure strength for Short FRSCs: Mullins effect

The last example illustrates that *both* mechanics and fiber statistics can significantly affect composite failure. Here we highlight fiber statistics on the failure process. We consider a soft unidirectional composite plate consisting of N parallel fibers with equal lengths L, Young's modulus E_j and cross-section area A_j (see Fig. 4 below). For the time being, we shall assume a short composite, that is, $L < l_T$. From the previous section, unbroken fibers are to an excellent approximation under ELS. The strength of these fibers, s_j , $1 \le j \le N$, in units of stress, are assumed to be independent and identically distributed random variables obeying Weibull statistics, that is, the probability of failure is given by (13). In the following, we assume s_j are arranged in increasing order, that is, $s_{j-1} < s_j$.

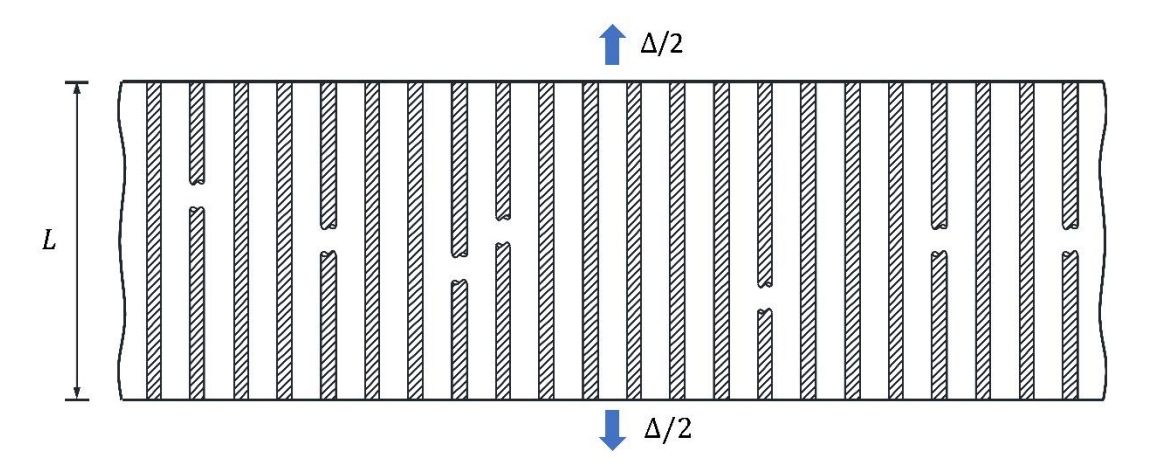


Fig. 4. A composite of N parallel fibers (shaded) with length L bonded to a soft matrix (white) in a displacement-controlled tension test.

Consider a displacement-controlled test where the composite plate is held between rigid grips and the grips are pulled apart by imposing a vertical displacement of $\pm \Delta/2$ (see Fig. 4). Before loading, all fibers are intact. As the sample is displaced to some $\Delta = \Delta_1$, the weakest fiber (first fiber) fails first. Because of equal load sharing, the stress along every fiber is uniform and hence the break can occur any place along the fiber. Once a fiber breaks, the *entire segment* of the fiber unloads (since $L < l_T$) rapidly so the energy loss is $\frac{E_f}{2} \left(\frac{\Delta_1}{L}\right)^2 A_f L$. In a displacement-controlled test where the composite is held between rigid grips, the stiffness of the composite is the sum of the stiffness of the total number of unbroken fibers. For example, just before the first fiber breaks, the total load in the composite is $NE_f A_f \Delta_1 / L$. After breaking, the load drops by exactly $E_f A_f \Delta_1 / L$. When i out of N fibers are broken, the stiffness of the composite is

$$k_{N-i} = (N-i)A_f E_f / L, \tag{15}$$

and the total load is related to the applied displacement Δ by

$$P_{i}(\Delta) = k_{N-i}\Delta . \tag{16}$$

Equation (16) holds before the next (i+1)-th fiber breaks.

The *nominal or composite stress* σ is the total force P divided by the total cross-sectional area of the fibers NA_j (the extreme softness of the matrix allows us to neglect the load carried by it). Just before and after the i-th fiber breaks where the displacements are both $\Delta = \Delta_i$, the nominal stresses are

$$\sigma_i^- = \frac{P_{i-1}(\Delta_i)}{NA_f} = \frac{(N-i+1)E_f\Delta_i/L}{N} = \frac{(N-i+1)E_f\varepsilon_i}{N} , \qquad (17a)$$

$$\sigma_i^+ = \frac{P_i(\Delta_i)}{NA_f} = \frac{(N-i)E_f\Delta_i/L}{N} = \frac{(N-i)E_f\varepsilon_i}{N} , \qquad (17b)$$

where $\varepsilon_i = \Delta_i/L$ is the composite strain and the superscripts '-' and '+' express the stress just before and just after the *i*-th fiber break. By (17b), the fraction of surviving fibers (N-i)/N decreases with *i* and eventually reaches zero when i = N. On the other hand, the applied strain ε_i or Δ_i increases with *i*, so there must exist a maximum load P_{max} or maximum nominal stress σ_{max} at some $i = i_{\text{max}} < N$. From (17a), the maximum nominal or composite stress is simply

$$\sigma_{\max} = \frac{P_{\max}}{NA_f} = \max \left\{ s_1, \frac{N-1}{N} s_2, \dots, \frac{2}{N} s_{N-1}, \frac{1}{N} s_N \right\},$$
(18)

where we have used $E_f \varepsilon_i = s_i$. The total energy dissipated for a composite with i fiber breaks, Λ_i , is

$$\Lambda_i = \frac{A_f L}{2E_f} \sum_{j=1}^i s_j^2 . \tag{19}$$

The *energy density* (energy per unit volume) dissipated in a displacement-controlled test is the area under the nominal stress σ versus strain ε curve. This energy density is often thought of as being the *work of extension* (per unit volume).

Since the nominal stress drops every time a fiber breaks, the nominal stress-strain curve of this composite is saw-tooth like. Fig. 5 plots this curve for a composite consisting of 5 fibers (N = 5). To illustrate this idea, the failure stresses of the fibers are chosen, in some convenient units, to be $s_j = j$, j = 1,2,3,4,5 respectively. Also, the fiber cross-sectional area A_j is 1 in some chosen unit. The first fiber breaks when $\sigma = s_1 = 1$ unit. Immediately after the break, the load drops to 4 and the nominal stress drops to 4/5 (see (17b)). To break the second fiber, the stress on the unbroken fibers has to increase to 2, which requires a total load of 8 or a nominal stress of 8/5. Immediately after the second fiber fails, the load drops by 2, and the nominal stress suddenly decrease from 8/5 to 6/5. Following this line of reasoning, one sees that for this particular specimen the peak load is 9, corresponding to a peak nominal stress of 9/5. The situation is shown in Fig. 5.

If we unload and reload the composite at a point on the stress/strain curve without exceeding the stress where the next weakest fiber fails (e.g., $\sigma < 9/5$), then the composite is *linearly elastic* with a reduced modulus. This is illustrated in Fig. 5. Here the red dotted line illustrates the path taken during unloading/reloading after the second fiber fails. The modulus for this case reduces by the factor of 3/5. This behavior is identical to the *Mullins effect* in rubber [37] and in DN hydrogels [38,39]. Here we note the close analogy with DN gels. In DN gels, it is the breaking of the sacrificial bonds in the stiff network that dissipates energy and reduces the gel modulus. In

general, the stress and strain curve in Fig. 5 will *vary* from sample to sample since the fiber breaking stress is random. In the following, mean nominal stress is defined as the nominal stress averaged over a large number of identical samples. Finally, it should be noted that the Mullins effect is a characteristic of FRP composites with *elastic* matrices and does not depend on the whether or not the composites are short or long.

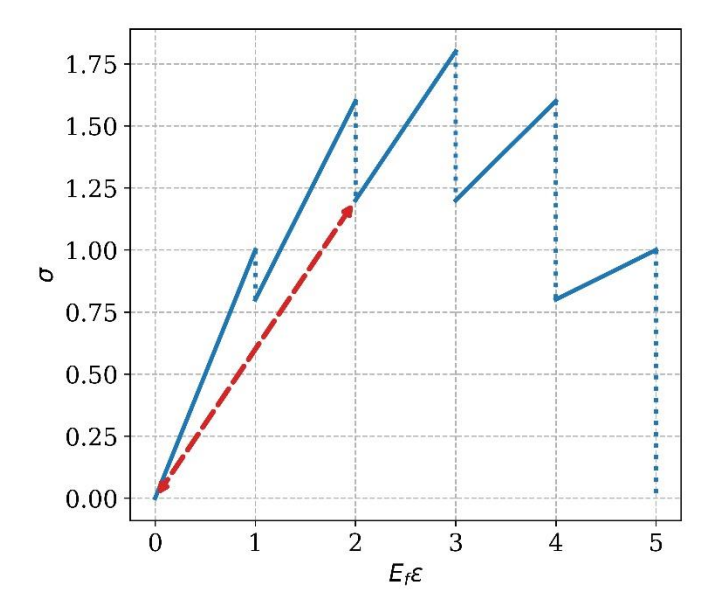


Fig. 5. A composite consisting of 5 fibers under ELS. The fiber strengths are 1, 2, 3, 4, and 5. After the second fiber breaks, if one unloads, then the sample unloads along the red line with reduced modulus. If one stops unloading at any point on the red line and reloads, the stress and strain follows the red line as long as the maximum load is below the failure load of the third fiber.

3.3 Failure stress and strain for short composites

Fig. 5 is for a small number of fibers. For large N and fibers that obey Weibull statistics, Daniels theory [26] shows that the mean nominal stress $\bar{\sigma}$ and the applied strain ε is:

$$\bar{\sigma} = E_f \varepsilon \exp \left| -\left(E_f \varepsilon / \sigma_L \right)^{\rho} \right|. \tag{20}$$

In addition, Daniels shows that the failure strength of an ELS bundle consisting of a large number of fibers of equal length L is *normally* distributed. Specifically, the failure probability $G(\sigma, L)$ that the composite fails for a nominal stress less than or equal to σ is

$$G(\sigma, L, N) = \Phi\left(\frac{\sigma - \overline{\sigma}_{\text{max}}}{\gamma_N^*}\right), \quad \Phi(z) = \frac{1}{\sqrt{2\pi}} \int_{-\infty}^{z} e^{-r^2/2} dr , \qquad (21)$$

where $\bar{\sigma}_{max}$ is the mean strength of the composite and γ_N^* is the standard deviation. In general, $\bar{\sigma}_{max}$ and γ_N^* depend on fiber statistics and bundle size. Using the Weibull model, Coleman [40] showed that

$$\bar{\sigma}_{\text{max}} = \sigma_L \rho^{-1/\rho} e^{-1/\rho}, \tag{22a}$$

$$\gamma_N^* = \frac{\sigma_L}{\sqrt{N}} \rho^{-1/\rho} \sqrt{e^{-1/\rho} \left(1 - e^{-1/\rho}\right)}$$
 (22b)

Note that the failure statistics of the composite is normal or Gaussian and is not the same as the failure statistics of its constituents (Weibull).

3.4 Energy Dissipation for short composites

An important consequence of the Mullins effect is that the energy dissipated by hysteresis in a cyclic test is the sum of the energies release by sudden unloading of broken fibers. In a displacement-controlled test, the sample fails in a stable fashion, and the total mean energy loss per unit volume of the composite (for $N \to \infty$), W_{loss}^D , is given by the integral under the stress-strain curve given by (20). For short composites where $L < l_T$,

$$W_{loss}^{D} = \frac{1}{E_{f}} \int_{0}^{\infty} s e^{-(s/\sigma_{L})^{\rho}} ds = \frac{\sigma_{L}^{2}}{E_{f}} \int_{0}^{\infty} x e^{-x^{\rho}} dx = \frac{\sigma_{L}^{2}}{\rho E_{f}} \int_{0}^{\infty} q^{(2/\rho)-1} e^{-q} dq = \frac{\sigma_{L}^{2}}{\rho E_{f}} \Gamma(2/\rho).$$
 (23a)

The superscript 'D' indicates it is displacement controlled. Equation (23a) shows that the mean energy loss density or work of extension depends on the shape parameter ρ . Using the properties of Gamma function, W_{loss}^D for large and small shape parameter ρ is:

$$W_{loss}^{D} = \frac{\sigma_{L}^{2}}{\rho E_{f}} \Gamma(2/\rho) = \begin{cases} \sigma_{L}^{2}/2E_{f} & \rho \to \infty \\ \frac{\sigma_{L}^{2}}{E_{f}} \sqrt{\frac{\pi}{\rho}} \exp\left[\frac{2}{\rho} \left(-1 + \ln\left(\frac{2}{\rho}\right)\right)\right] \to \infty & \rho \to 0 \end{cases}$$
(23b,c)

As expected, for large shape parameters, (23b) shows that the loss energy density is given by the *standard* elasticity solution where all fibers fails at the same stress. However, as the shape parameter approaches zero (fibers with extreme variability), the energy density increases and approaches infinity. In this regime, energy loss is dominated by fibers with high strength. Interestingly, the pre-factor in the loss energy density $\rho^{-1}\Gamma(2/\rho)$ has an absolute minimum of approximately 0.443 at $\rho = 4.33$.

In a force-controlled test, the composite fails at peak load, and the mean energy loss per unit volume is

$$W_{loss}^{F} = \frac{1}{E_{f}} \int_{0}^{\sigma_{L} \rho^{-1/\rho}} s e^{-(s/\sigma_{L})^{\rho}} ds = \frac{\sigma_{L}^{2}}{E_{f}} \int_{0}^{\rho^{-1/\rho}} x e^{-x^{\rho}} dx = \frac{\sigma_{L}^{2}}{\rho E_{f}} \int_{0}^{1/\rho} q^{(2/\rho)-1} e^{-q} dq = \frac{\sigma_{L}^{2}}{\rho E_{f}} \gamma \left(\frac{2}{\rho}, \frac{1}{\rho}\right). \tag{24}$$

where γ is the Incomplete Gamma function [41], and the superscript 'F' indicates it is force-controlled. Fig. 6 plots the normalized mean energy loss function versus the shape parameter ρ .

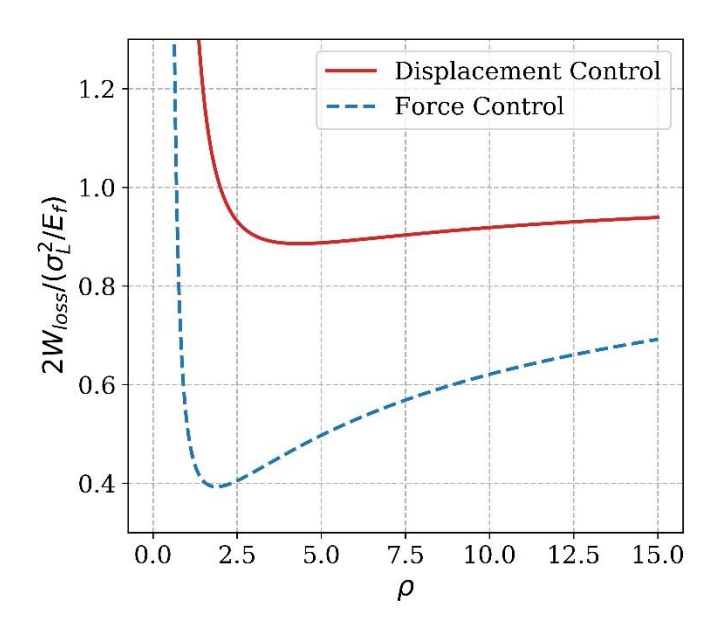


Fig. 6. Normalized energy loss per unit volume of a short composite versus the Weibull shape parameter. For very large ρ (not shown), both curves approach 1. The solid line is for displacement control whereas the dotted line is for force controlled.

3.5 Brittle-Ductile transition

Plots of stress $\bar{\sigma}$ versus strain ε for different shape parameters (20) is shown in Fig. 7 below. A simple calculation using (22a) shows that the *minimum* mean failure stress $\bar{\sigma}_{max}$ occurs at $\rho=1$. For large ρ , failure is brittle as the load drops abruptly after the peak load. For small ρ , the composite exhibits a stress-strain behavior similar to ductile metals and DN gels which yield and soften after yield. Fig. 7 shows that this ductile and brittle transition can be controlled by fiber statistics. To check our analytic result (20) which is strictly valid for a very large number of fibers, we generate random variables following a Weibull distribution with different shape parameters ρ , and use the strategy in section 3.2 to obtain the stress-strain curve of a finite composite where N=5000. Fig. 7 plots the normalized nominal stress-strain curve for different shape parameters. Details on simulations are given in the Supporting Information (SI).

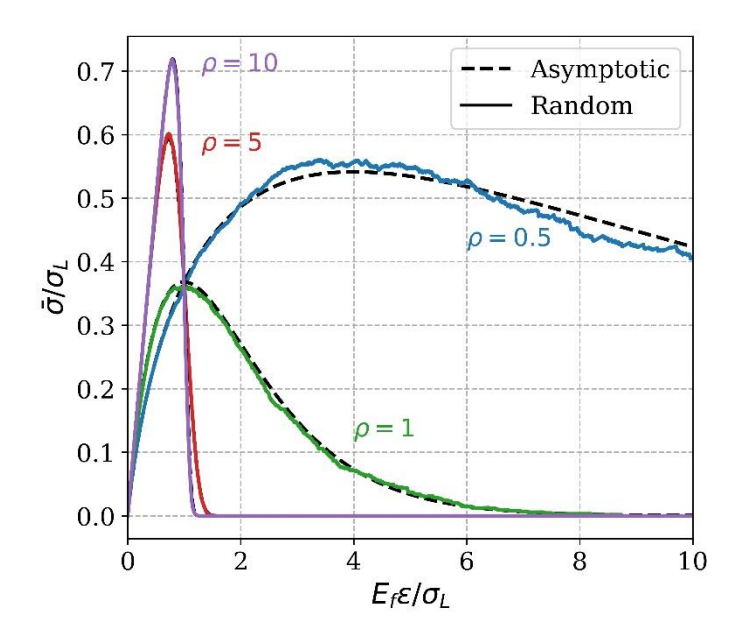


Fig. 7. Normalized mean nominal stress $\bar{\sigma}/\sigma_L$ versus $E_f \varepsilon$ where ε is the strain imposed on the short composite. The mean stress is normalized by σ_L and the strain is normalized by E_f/σ_L . The dotted curve is the asymptotic result given by (20) ($N \to \infty$). The solid lines are obtained by simulation.

Percentage of fiber failure and loss of stiffness

The strength distribution of fibers is reflected by the percentage of fiber failure at the peak load. Equation (15) shows that the loss of stiffness of the composite is directly proportional to the number of broken fibers which we denote by i. For a large number of fibers, the ratio of the composite stiffness is $k_{N-i}/k_N = (N-i)/N$ $= \overline{\sigma}(\varepsilon)/E_f\varepsilon$. This ratio can be computed using (20):

$$k_{N-i} / k_N = (N-i) / N = \exp \left[-\left(E_f \varepsilon / \sigma_L \right)^{\rho} \right] \Rightarrow i / N = 1 - \exp \left[-\left(E_f \varepsilon / \sigma_L \right)^{\rho} \right]$$
(25a)

In particular, at peak load where $\varepsilon = \rho^{-1/\rho} \sigma_L / E_f$ the fraction of fiber break at peak load, denoted by $(i/N)_{peak}$ is

$$(i/N)_{peak} = 1 - e^{-1/\rho}$$
 (25b)

As expected, for a large shape parameter, that is, $\rho >> 1$, none of the fibers break before the peak load. However, for $\rho = 9$, only 10% of the fibers break at peak load. In general, the fraction of fiber break at peak load is a monotonic decreasing function of ρ , as shown in Fig. 8.

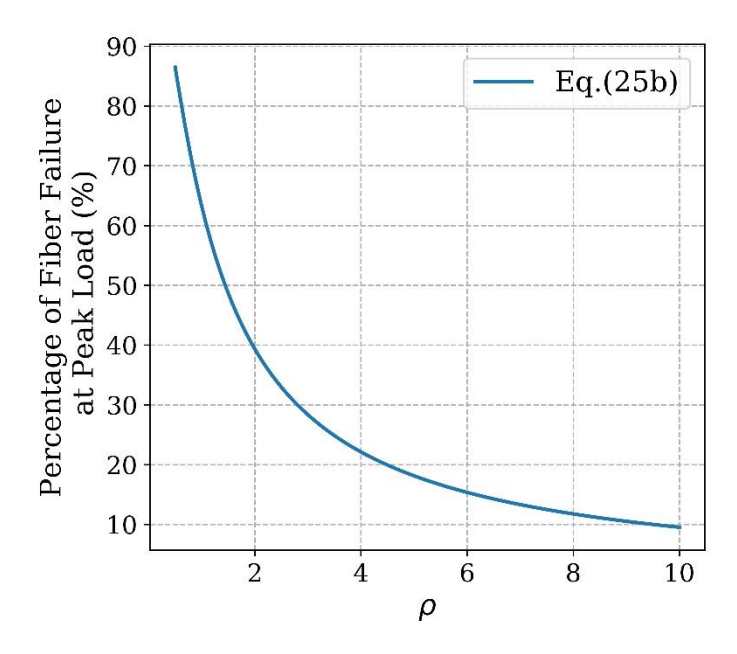


Fig. 8. The percentage of fiber break at peak load versus Weibull shape parameter.

3.6 Failure of large composites $(L > l_T)$

Next we consider the failure of "large" composites consisting of N parallel fibers with length $L > l_T$. As before, these fibers are assumed to be perfectly bonded to the soft elastic matrix. Similar to the previous example, the initial state of the composite is assumed to be free of cracks or fiber breaks. Upon loading, fiber break occurs at random locations. Unlike the previous section which considers short composites, the fibers in the composite here are NOT under ELS once fibers break. Indeed, the stress on a broken fiber can recover at distance sufficiently far from the break, so certain sections of a broken fiber can carry the full load. This means that multiple breaks can occur along a single fiber. Following Rosen [27], we model the composite as a chain of $m = L/l_T$ "short" ELS composites, each having N fiber elements of characteristic length equal to the load transfer length $l_{\rm T}$, and with the tensile load-carrying capability of the matrix being neglected. Rosen's model is often referred to in the literature to as the chain-of-ELS-bundles model, where in our context each bundle is understood to be short composite. We denote the composites strength of each short composite by S_1, S_2, \dots, S_m respectively. We assume that these strengths are independent and identically distributed random variables with common distribution function given by $G(\sigma, l_T, N)$ in (22). This assumption implies that the strength of the chain is $\min\{S_1, S_2, \dots, S_m\}$ meaning that the chain fails if the weakest short composite (or bundle) fails. The failure probability is $1-\left[1-G(\sigma,l_T,N)\right]^m$. Thus, the probability function H for the strength of the chain or composite strength is

$$H(N,m,\sigma) = 1 - \left[1 - G(\sigma,l_T,N)\right]^m. \tag{26}$$

For large number of fibers, the mean strength $\bar{\sigma}_{max}(m)$ of a chain made up of m bundles can be computed using (26) and is found to be (see SI)

$$\bar{\sigma}_{\max}(m) = \bar{\sigma}_{\max}(m=1) + \sqrt{2}\gamma_N^* \omega_m, \qquad (27a)$$

where

$$\omega_{m} = \frac{m}{\sqrt{\pi}} \int_{-\infty}^{\infty} \left[erfc(\eta) / 2 \right]^{m-1} e^{-\eta^{2}} \eta d\eta < 0.$$
 (27b)

Here m=1 means evaluating quantities at the length $L=l_T$ (the composite in this case is a bundle under ELS). Hence $\overline{\sigma}_{\max}\left(m=1\right)$ can be obtained by setting σ_L to be σ_{l_T} in (22a,b). It should be noted that the second term in (27a) is negative (see SI), meaning that the mean strength decreases as the size of the composite (m) increases. A plot of $\overline{\sigma}_{\max}\left(m\right)$ versus ρ for N=1000 is shown in Fig. 9(a). The minimum occurs at $\rho\sim 1$. Fig. 9(b) plots the percentage change of $\overline{\sigma}_{\max}\left(m\right)$, i.e., $\frac{\overline{\sigma}_{\max}\left(m\right)-\overline{\sigma}_{\max}\left(m=1\right)}{\overline{\sigma}_{\max}\left(m=1\right)}\times 100$ versus the Weibull shape parameter. Since ρ for most fibers is between 3 and 12, the percentage change is less than 5% for m=100. Note, for FRSCs, m=100 corresponds to a composite size on the order of 2 meters.

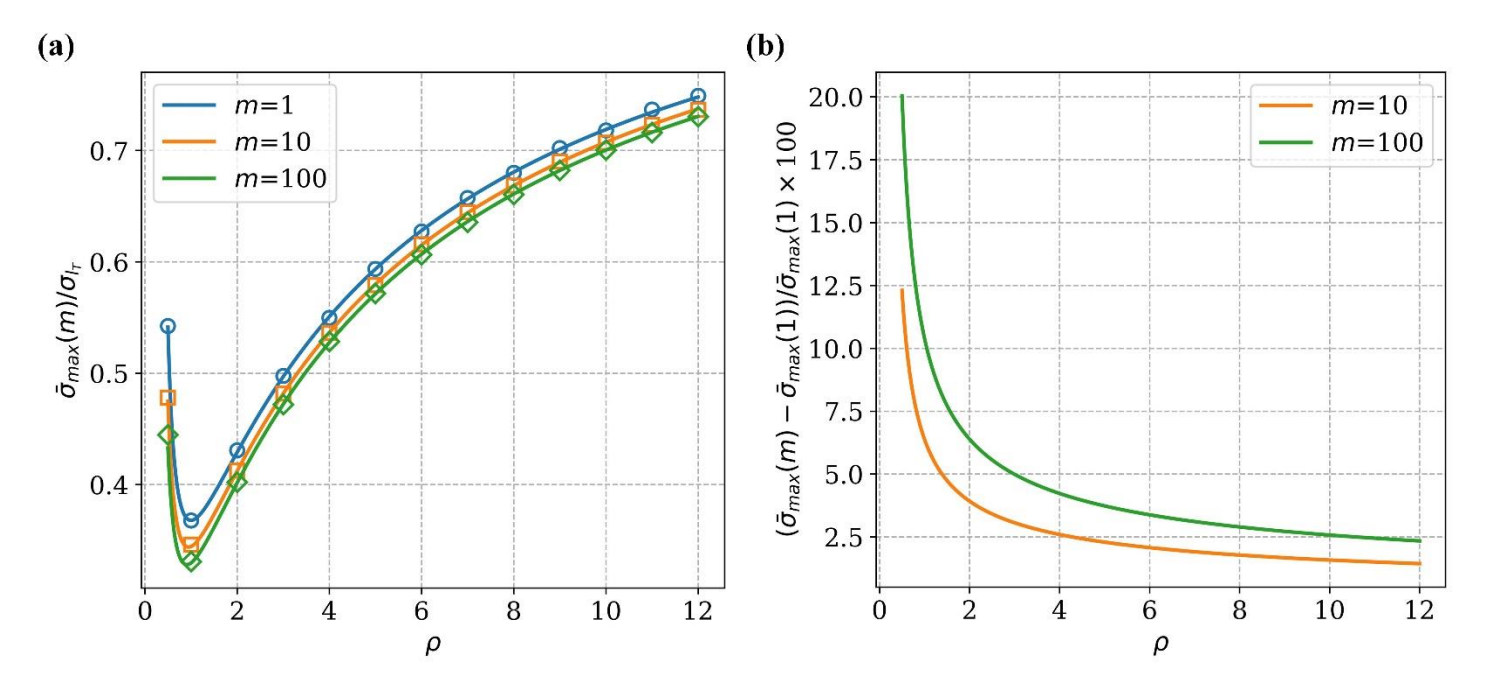


Fig. 9. (a) $\bar{\sigma}_{\max}(m)/\sigma_{l_T}$ versus the shape parameter ρ , the solid lines are equations (27a,b) and the symbols are simulation results. (b) Percentage difference between the mean strength for a chain of m bundles and a single bundle $\frac{\bar{\sigma}_{\max}(m) - \bar{\sigma}_{\max}(m=1)}{\bar{\sigma}_{\max}(m=1)} \times 100$ versus ρ .

To compute the mean energy density loss function, we need an expression similar to (20) for the mean stress versus strain. Unfortunately, we have not been able to derive such an expression. Hence, we use simulations to find this stress-strain curve. We index an element (bundle) of the chain by i, $(i = 1, 2, \dots, m)$ and denote the stress-strain curve of the i-th element or bundle by $C^{(i)}$. The procedure is as follows. In step 1, we numerically generate m stress-strain curves $C^{(i)}$, $(i = 1, 2, \dots, m)$. In step 2, we obtain a stress-strain curve by finding the lower boundary of all $C^{(i)}$. We repeat these two steps 1000 times and compute the mean of all resulting stress-strain curves and we denote this curve by C^* . In all our simulations, the number of fibers is chosen to be N = 1000. More details can be found in the SI. Finally, it should be noted that if the number of fibers N goes to infinity, then each $C^{(i)}$ is given exactly by (20). Indeed, since γ_N^* goes to zero as N goes to infinity, $\overline{\sigma}_{\max}(m) \to \overline{\sigma}_{\max}(m = 1)$ for any finite chain.

In the SI, we show that a good approximation for the mean energy density in a force-controlled test is to rescale $\bar{\sigma}_{\max}(m)$ by dividing it by $\bar{\sigma}_{\max}(m=1)$, i.e., $\bar{\sigma}_{\max}(m)/\bar{\sigma}_{\max}(m=1)$. We expect this factor to be less than 1. For force-controlled test (denote by the superscript F), we found numerically that

$$W_{loss}^{F}(m) = \frac{\overline{\sigma}_{max}(m)}{\overline{\sigma}_{max}(m=1)} W_{loss}^{F}(m=1).$$
(28)

For displacement-controlled test, the mean energy loss per unit volume is approximately:

$$W_{loss}^{D}\left(m\right) = W_{loss}^{D}\left(m=1\right) + \frac{\overline{\sigma}_{max}\left(m\right) - \overline{\sigma}_{max}\left(m=1\right)}{\overline{\sigma}_{max}\left(m=1\right)} W_{loss}^{F}\left(m=1\right) - \left[\overline{\sigma}_{max}\left(m=1\right) - \overline{\sigma}_{max}\left(m\right)\right] \left(\eta - \frac{\sigma_{l_{T}}\rho^{-1/\rho}}{E_{f}}\right), \quad (29a)$$

where η is the largest root of the equation

$$\overline{\sigma}_{\max}(m=1) - \overline{\sigma}_{\max}(m) = E_f \eta \exp \left[-\left(E_f \eta / \sigma_0 \right)^{\rho} \right]. \tag{29b}$$

It should be noted that the refinements offered by (28) and (29a, b) are for m > 100. For m < 100, the mean strength and energy density for large composites can be well approximated by (22-24). This means that the mean strength of reasonably large composites ($m \le 100$) are roughly the same as short composites (i.e., one bundle). This result is relevant since it highlights the important role of the soft matrix in maintaining the strength of the composite. Indeed, if the soft matrix were replaced by air, the strength of the composite would have gone down by a factor of $(l_T/l)^{1/\rho} = m^{-1/\rho}$. For example, if we take $\rho = 3$ and m = 100, the mean strength decreases by 78%. As demonstrated by King et al. [4], neat composites without a soft matrix has significantly less strength and energy dissipation. However, it must be emphasized that King et al.'s neat composite is a woven fabric which

has much more complicated micro-mechanics than the unidirectional composites in this study. Here we emphasized that the Rosen model of failure is very crude in this context. This model is likely going to break down before the peak load. We will discuss the limitation of this model in the discussion.

4. Fracture mechanics of FRSCs

Traditional fracture testing of homogeneous materials is usually done by loading a sample containing a *precrack* until crack growth occurs. From such tests one determines a quantity called fracture toughness which is supposed to be independent of specimen geometry. For fiber-reinforced composites, such tests have limited utility since cracks in these composites occur due to fiber breaks and their spatial positions are randomly distributed. It is only at the very end of the composite's life that fiber breaks coalescence into a large "crack" failing the sample. Indeed, fracture rarely occurs on a single plane – the crack path is tortuous. Therefore, reliable predictions based on fracture testing in composites with a pre-crack should be interpreted with great care.

As an example, let us compare two pure shear crack samples with a *semi-infinite* crack (see Fig. 2). The first sample, Sample 1, has a height $L_1 \ll l_T$ and the second sample, Sample 2, has $L_2 \gg l_T$. In the short fiber specimen (Sample 1), the fibers are stronger by a factor of $\left(L_2 / L_1\right)^{1/\rho}$, and all the unbroken fibers are under ELS. As discussed previously, the failure mode of the shorter fiber specimen is highly diffuse and random – there is no crack growth and no well-defined fracture plane. The specimen fails in two phases: in the first, fibers fail in random locations dictated by flaw statistics. At the end of the first phase, almost all the fibers fail. In a traditional composite, the composite will fail virtually immediately as the load drops to almost zero, and the matrix has no load-carrying ability thereafter. However, in a displacement-controlled test, the FRSCs will not fail even though it suffers a huge reduction in stiffness. This is because the soft matrix is very tough and can sustain very large strains before failure. The second phase of failure is dominated by matrix failure and fiber pull-out. The mean failure strength and failure strain in the first phase is given by (22a, b) respectively with $L = 2L_1$.

We next estimate the fracture energy to fail Sample 1. We could have divided the fracture energy by the total uncracked area of the sample and call this the fracture energy per unit area, G_f . However, as noted earlier, G_f has nothing to do with the critical energy release rate since the fibers ahead of the crack is subjected to ELS. In this regime the crack plays no role. Because of this, the appropriate indicator is the work of extension W_f which is the energy needed to fail a unit volume of the sample. To estimate W_f , we first find the energy per unit volume dissipated by the sudden unloading of fibers in an ELS sample. Our previous analysis (see (23a)) shows that

$$W_{loss}^{D} = \frac{\sigma_{L}^{2}}{\rho E_{f}} \Gamma(2/\rho). \tag{30}$$

However, there is an *additional* contribution to W_J . For the specimen to fail, the matrix has to fail. Since the matrix can sustain very large stretches before failure, it is possible that substantial additional strain is needed to fail the composite, even though the load has dropped drastically because the fibers are not carrying load. In this regime the specimen loses the constraint provided by the intact fibers and is subjected to very large deformation. As a result, the stress state on the matrix is highly complex and the shear-lag model is not applicable. In this regime, a possible failure mode is pulling out of broken fibers from the matrix. Clearly, this process also contributes to energy dissipation. We denote the energy contribution (per unit volume) due to pull-out by $W_{pullout}$. We roughly estimate $W_{pullout}$ by assuming the location of fiber breaks follows a uniform distribution, so that the mean distance of breaks measured from the center line of specimen or the crack plane (y = 0) is $L_1/2$; that is, on average, the fiber pull-out length is approximately $L_1/2$. We further assume fiber pull-out is achieved by propagating a shear crack in the *matrix* and that the soft matrix has a fracture toughness of G_m , which for tough soft gels, is on the order of 3000 to 5000 J/m². This assumption is consistent with the very limited experimental data on the mechanism of fiber pull-out in FRSCs. In tear tests performed on a woven glass fabric impregnated with a soft PA gel, it was found that fiber pull-out results from matrix failure rather than the growth of an interface crack [4]. Thus, an upper estimate of the contribution to the work of extension due to fiber pull-out is:

$$W_{pullout} \approx \rho_f G_m L_1 c / 2, \tag{31}$$

where c is the circumference of the matrix crack and ρ_f is the number of fibers per unit volume. A rough estimate is $c \approx 4h$, where h is the radius of the fiber. Substituting this into (31),

$$W_{pullout} \approx 2\rho_f G_m L_1 h. \tag{32}$$

Combining (30) and (32), the work of extension W_t is

$$W_f = W_{loss}^D + W_{pullout} = \frac{\sigma_L^2}{\rho E_f} \Gamma(2/\rho) + 2\rho_f G_m L_1 h.$$
(33)

It is important to note that W_f is specimen *size dependent* since both W_{loss} and $W_{pullout}$ depends on the length of fibers. The uncertainty in (33) is $W_{pullout}$ – it is possible that (33) overestimates the energy density. For example, the matrix can fail in a different way due to the high constraint of the fibers.

An order of magnitude estimate can be made on W_{loss}^D and $W_{pullout}$ based on the experiments of Huang et al. [6]. A rough estimate of W_{loss}^D is about $3\times10^7\,\mathrm{J/m^3}$ where we have used $\sigma_{L_1}=240\,\mathrm{MPa}$ and $E_f=5.5\,\mathrm{GPa}$, with ρ sufficiently large so that $\rho^{-1}\Gamma(2/\rho)\approx1/2$. To estimate $W_{pullout}$, we use $G_m=3.5\times10^3\,\mathrm{J/m^2}$ for the fracture

energy of the PA gel [6] $\rho_f = 6.5 \times 10^9 \,\mathrm{m}^{-3}$, $L_1 = 20 \,\mathrm{mm}$, $h = 7 \,\mu\mathrm{m}$, resulting in $W_{pullout} = 6.4 \times 10^6 \,\mathrm{J/m}^3$. Note that the energy dissipated from fiber breakage and from pull-out is roughly on the same order of magnitude. This result is consistent with recent tearing test performed on the weaved glass fiber composite [6]. Here we mention the recent work by Wang et al. [42] who use a very different system, and find that the energy dissipated in their composite correlates well with the energy release by the sudden breaking of fibers.

Next, consider the case of a "large" composite $L_2 > l_T$ with a *long pre-crack* (Sample 2). For this case the fibers are *weaker*. As shown in section 2.7, stresses are *concentrated* at the crack tip when $L_2 / l_T >> 1$. Hui et al. [31] have recently shown that the fiber stress in the specimen in Fig. 2 can be accurately predicted by:

$$\sigma_f \equiv C_{22}\varepsilon \operatorname{Re} \left\{ \sqrt{\frac{1}{1 - \exp(-\pi \alpha z / L_2)}} \right\}, \quad \alpha = \sqrt{\frac{C_{22}}{C_{12}}} >> 1,$$
(34a)

where

$$\alpha z / L_2 = (s - 2/3) / \overline{L}_2 + i \overline{y} / \overline{L}_2, \quad i = \sqrt{-1}.$$

$$(34b)$$

In (34a,b), $\bar{y} = y/l_T$, $\bar{L}_2 = L_2/l_T$ and Re denotes the real part of a complex number. Recall that s denotes the fiber number directly ahead of the crack tip. Here we note that the stresses given by the continuum crack solution (34a) have a square root singularity as one approach the crack tip. Since the continuum solution does not account for the discrete geometry, the position of the crack tip must be interpreted carefully so the stress on the fiber calculated using the continuum model is in close agreement with the DSLM. In our previous work [31], we found that this condition is satisfied when z is related to the fiber number s by (34b). The accuracy of our analytic results given by (34a,b) is verified by a finite element method. Details are given in the SI.

Note $L_2/l_T >> 1$ implies that, near the crack tip, (34a) can be approximated by:

$$\sigma_f \approx C_{22} \varepsilon \operatorname{Re} \sqrt{\frac{1}{\pi \alpha z / L_2}}$$
 (35)

This is because near the crack tip, $\pi\alpha z/L_2$ is small, hence $1-\exp(-\pi\alpha z/L_2)\approx \pi\alpha z/L_2$. The factor $K_I\equiv C_{22}\varepsilon\sqrt{2L_2/\alpha}$ in (35) corresponds to the *stress intensity factor* of the crack. Because the factor $\alpha>>1$, the stress intensity factor is small unless the specimen is very large – reflecting the flaw insensitivity of soft composites. For large enough specimens, it is possible that failure occurs by the growth of the preexisting crack. However, even in this regime, the crack does not propagate along a well-defined plane (e.g. the plane containing the initial pre-crack). This is because the strength of fibers is statistically distributed and the stress acting on all fibers are finite. Hence, during loading, a diffuse zone of fiber breakage forms and engulfs the crack tip. We shall call this the damage zone.

Let us estimate the shape of the damage zone Ω_d by setting σ_f in (34a) to σ_{L_2} , the scale parameter for the fibers in Sample 2. In other words, we determine the boundary of the damage zone by finding where fiber stress reaches σ_{L_2} , which is close to the mean strength of the fiber. For each value of the applied nominal stress $C_{22} \varepsilon$, we solve (34a) to find the location z where $\sigma_f = \sigma_{L_2}$. This procedure generates a curve which is the boundary of $\Omega_{\scriptscriptstyle d}$ for the applied strain. Fig. 10 plots the shape of the damage zone $\Omega_{\scriptscriptstyle d}$ for specimens with $\overline{L}_2 \equiv L_2 / l_T = 5{,}10{,}100$ for different applies strains. The vertical axis \overline{y} in Fig. 10 is in the fiber direction and distance on this axis is normalized by l_{τ} . The horizontal axis is s. Recall integer value of s represent a fiber and in Fig. 10 fibers are indicated by gray bars. As expected, increasing the applied strain increases the size of the damage zone. Since the continuum solution is meaningless if s < 1 (Ω_d has to contain at least one fiber), we do not plot any curve that is contained in a circle of radius 1 centered at the crack tip. This means excluding $\bar{L}_2 \leq 1$ (i.e., Sample 1) since for this case the stress concentration is so small that no damage zone will form until $C_{22}\varepsilon/\sigma_{L_2} \to 1$. Indeed, even for $\overline{L}_2 = 5$, the *smallest* damage zone (this damage zone contains *only* one fiber directly ahead of the crack tip) occurs at $C_{22} \varepsilon / \sigma_{L_2} = 0.5$. The stress concentration for the case of $\bar{L}_2 = 10$ is still not sufficient to apply LEFM, since the smallest damage zone appears at $C_{22}\varepsilon$ / σ_{L_2} = 0.4 . For \overline{L}_2 = 100 , the stress concentration is now large enough, so the smallest damage zone occurs at $C_{22}\varepsilon/\sigma_{L_2}=0.1$. This is the regime where LEFM is applicable. Recall for LEFM to be applicable, the following constraints should be satisfied: (1) the applied stress should be much less than the fiber breaking stress; (2) the damage zone should be large enough to include relevant micromechanics but small enough so that the singular field still dominates. For our case, the first condition is satisfied if

$$C_{22}\varepsilon \ll \sigma_{L_2}. \tag{36}$$

In other words, the applied nominal stress must be much less than the mean stress for fiber break. The second condition requires that there is at least one fiber inside the damage zone and $\overline{L}_2 \equiv L_2/l_T >> 1$. A necessary consequence of LEFM is that the shape of the damage zone should be determined by the asymptotic field (36), which can be rewritten as:

$$R = \frac{\overline{L}}{2\pi} \left(\frac{C_{22}\varepsilon}{\sigma_l} \right)^2 \left(1 + \cos \theta \right) \quad \text{where } R = \sqrt{\left(s - 2/3 \right)^2 + \overline{y}^2} , \cos \theta = \frac{s - 2/3}{R} . \tag{37}$$

Equation (37) indicates that the shape of the damage zone is a limacon. Shapes of the damage zone predicted by the asymptotic field (35) are plotted as dashed lines in Fig. 10 for comparison with the full field solution.

The results in Fig. 10 shows that fracture mechanics is not applicable to specimens with $\overline{L} \leq 10$. For $\overline{L} = 100$, deviation occurs when $C_{22}\varepsilon/\sigma_{L_2} > 0.3$ as the asymptotic solution (35) underestimates the size of the damage zone. Note that the damage zone for $C_{22}\varepsilon/\sigma_{l} = 0.3$ contains only 3 fibers with lengths between 1.7 to $1.9\,l_T$. Unless these fibers all fail on the crack plane, which is unlikely, the size of the damage zone may be too small to fail the sample. Thus, failure of the sample would require larger values of $C_{22}\varepsilon$; however, in this case the damage is no longer controlled by the elastic "singular" field, and hence the amount of damage will depend on the specimen geometry. As a result, the concept of fracture toughness breaks down. Surprisingly, the shape and size of the damage zone is reasonably well approximated by the asymptotic theory even for large values of $C_{22}\varepsilon/\sigma_{L_2}$ where LEFM theory is expected to breakdown.

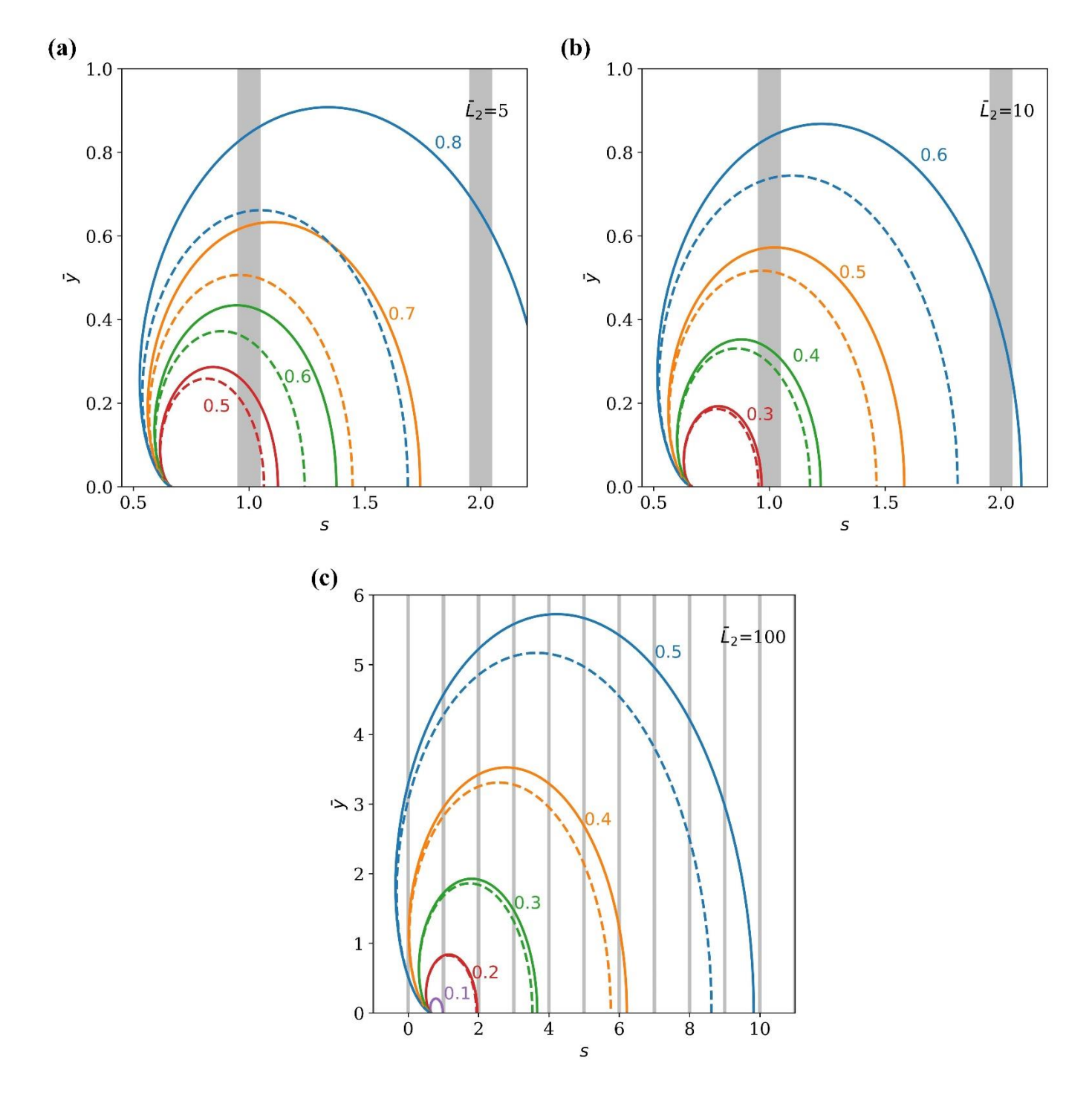


Fig. 10. Shapes of damage zone at different nominal stress levels $C_{22}\varepsilon/\sigma_{L_2}$ for different normalized fiber lengths (a): $\overline{L}_2 = 5$, (b): $\overline{L}_2 = 10$, (c): $\overline{L}_2 = 100$. Solids lines are generated by solving (34a) with $\sigma_f = \sigma_{L_2}$ and dotted lines are the asymptotic solution based on (35).

Let us consider the case of $\overline{L}_2 = 100$. The size of the damage zone (see Fig. 10(c)) for $C_{22}\varepsilon = 0.2\sigma_{L_2}$ engulfs one fiber directly ahead of the crack tip. This fiber is likely going to break somewhere inside the damage zone

and the crack can propagate by breaking one fiber at a time. The energy dissipated by propagating the crack a unit area is roughly

$$G \approx W_{loss}^D l_T \,, \tag{38}$$

the energy release by elastic unloading of fibers, where we have neglected the energy contribution due to fiber pull-out.

5. Summary and Discussion

We study the mechanical behavior of unidirectional FRSCs. Fibers are assumed to be well-bonded to the soft matrix and obey Weibull statistics. The long load transfer length in FRSCs means that the size of the composite (in our case the fiber length) is an important geometric parameter. We also highlight the relevance of fiber statistics to the failure strength and work of extension. Our main results can be summarized as follows:

- (a) The long load transfer length due to stiff fiber and soft matrix dramatically reduces stress concentration. Since stiff fibers store huge amounts of energy before they break and the length between breaks is on the order of the load transfer length, the energy dissipation due to fiber breaks is large.
- (b) FRSCs exhibit Mullins effect commonly observed in rubbers and DN gels.
- (c) The mean failure stress $\bar{\sigma}_{max}$ for composites with fiber less than 100 times its load transfer length is well approximated by the mean failure stress of a composite with fiber length equal to or less than the load transfer length, i.e., $\bar{\sigma}_{max} = \sigma_{l_T} \rho^{-1/\rho} e^{-1/\rho}$. However, this result can underestimate the composite strength since it is obtained using the chain-of-ELS-bundles model, which neglects interactions between fiber breaks in different sections (i.e., different bundles). However, a full-scale simulation without this assumption is an extremely difficult problem and is beyond the scope of this work.
- (d) A lower bound of work of extension is the energy loss due to fiber breaks. This energy density is given by (23a) or (24), with σ_L in these equations replaced by σ_{l_T} . This is a lower estimate since fiber pull-out due to matrix failure is not included. For tough soft matrices, the energy dissipation due to fiber pull-out can be quite significant and is on the same order of magnitude as the energy dissipated by fiber breaks. These results are consistent with the few experiments on soft composites. For example, Huang et al. [6] have found that fiber breakage and matrix failure contributed equally to energy dissipation of their woven fiber PA gel composite. Wang et al. [42] have made a model composite by bonding stiff polydimethylsiloxane (PDMS) fibers to a softer PDMS matrix and found that the toughness of the composite is much higher than its constituents. They attribute this increase in toughness to the release of strain energy associated with fiber breaks, which is consistent with our model.

- (e) In principle, the composite can exhibit a brittle to ductile transition when the shape parameter is smaller than one. In practice, shape parameter for fibers is usually greater than 3.
- (f) FRSCs are extremely flaw insensitive and fracture mechanics must be used with great care. Indeed, due to the long load transfer length, fracture of composites with pre-cracks are size/sample sensitive. The size dependence of fracture energy is demonstrated by recent tearing experiments by Huang et al. [5,6]. Their experiments indicated that the tearing energy is not a material property as it increases with the width of the composite (consisting of a glass fabric bonded to PA gel) until the width reaches and exceeds a load transfer length which is on the order of centimeters. This observation is again consistent with the model presented here.

It is important to note that our model assumes good adhesion between the fiber matrix interface. This is the case with the woven fiber PA gel composite [4,5]. In fact, the matrix/fiber interfaces are so strong that failure invariably occur in the matrix [6]. In contrast, the interfaces are very weak in the steel wool/gel composites of Illeperuma et al. [2], as a result, both composite strength and toughness are compromised.

There is a close connection between the DN gel discovered by Gong et al. [43] and FRSCs. The DN gel is a molecular soft composite since it is essentially a stiff polymer network embedded in a soft polymer network. Like FRSCs, DN gels exhibit the Mullins effect due to the breaking of the stiff network [38,39]. The energy loss of broken chains in the stiff network is analogous to the energy loss due to fiber breaks in FRSCs. However, unlike the highly aligned fibers in our unidirectional composite, the stiff network in DN gels is three dimensional with a spatial distribution of chemical crosslinks. As a result, the load transfer mechanics between the stiff network and the soft network is much more complex and is poorly understood. For example, the stiff network, being 3D, will not be under equal load sharing in the absence of the 2^{nd} network. It is interesting to note that, since the molecular weight between crosslinks in the DN gel is not a *fixed number*, the stretches needed to break chains in the stiff network is statistically distributed. To push the analogy further, this translates to very small Weibull parameter in our FRSCs. Indeed, the stress versus strain curve of DN gels exhibit yielding and softening behavior similar to that of FRSCs for $\rho = 0.45$. Here we note that tough DN gels typically exhibit a yield stress followed by necking. The stress strain curve often has a long plateau after the yield point before the network strain hardens [38,43,44]. Because the matrix is so soft in comparison with the fibers, this plateau and upturn of the stress-strain curve does not occur in our FRSCs.

Based on our model, we propose the following design criteria:

- (a) Use high strength fibers to increase energy dissipation W_{loss} .
- (b) Utilize fibers of appropriately long length, because fibers in short composites do not reach their maximum load bearing capability and toughness can also be compromised due to pull-out.
- (c) Ensure good interfacial adhesion to allow for effective load transfer.

(d) Incorporate an elastic matrix that is soft in small strains, but strain hardens rapidly at large strains.

The last criterion requires explanation. As mentioned at the end of Section 3, the Rosen model is crude and likely fails near the peak load. For a composite with a large number of fibers, the peak loads for different "short" composites or links are close to each other. This means that when the weakest link reaches the peak load, the next weakest link is not so far from it. This is particularly true if the number of fibers is large since in the limit of large number of fibers the variance vanishes. However, because the bundles are in series, this weaker link can never reach its peak load unless the matrix can take up some of the lost tensile load due to fiber breakage in the weakest link. Since the matrix is still highly constrained by the stiff fibers at peak load; and because it is so soft, the tension load carried by the matrix is negligibly small in comparison with the load loss due to the breaking of fibers. This means that next weakest link can never reach peak load unless two conditions are satisfied: (1) the volume fraction of fiber is sufficiently low (2) the matrix strain hardens substantially at larger strains. If these conditions are satisfied, then the soft composites can exhibit yield behavior since links can fail consecutively at increasing strains.

There are obvious limitations in our model. The matrix is assumed to be elastic, whereas many tough gels yields at moderate strains. Note this does not invalidate our analysis since the composite strain remains very small as long as a small fraction of fibers remain intact. However, large strains will affect how the composite fails, e.g. during fiber pull-out. Our micro-mechanical model for fiber pull-out is extremely crude since little is known about this mode of failure in FRSCs. To illustrate ideas, we confine our analysis to a simple geometry and the composite is subjected to uniaxial tension. For example, we do not consider 3D composite structures which are important for applications. Also, many hydrogels are viscoelastic [45] or even visco-plastic and this will affect load transfer between the fiber and matrix. We do not consider systems where debonding of the gel/fiber interface can occur near a fiber break. In these systems, the load transfer mechanics are more complex and fiber pull-out can occur prematurely before fibers can break if the interfaces are weak. Nevertheless, we believe that many of the fundamental issues are addressed and hope this work will stimulate interest in this emerging area.

Conflicts of interest

There are no conflicts to declare.

Acknowledgements

CYH acknowledge support by National Science Foundation (NSF), USA MoMS program under grant number 1903308. SLP acknowledges financial support from National Institute of Standards and Technology

under agreement ID 70NANB14H323. JPG and DRK acknowledge support by JSPS KAKENHI under grant number JP17H06144. JPG acknowledges the Institute for Chemical Reaction Design and Discovery (ICReDD), World Premier International Research Initiative (WPI), MEXT, Japan.

References

- [1] S. Sádaba, F. Martínez-Hergueta, C.S. Lopes, C. Gonzalez, J. LLorca, 10 Virtual testing of impact in fiber reinforced laminates, in: P.W.R. Beaumont, C. Soutis, A. Hodzic (Eds.), Structural Integrity and Durability of Advanced Composites, Woodhead Publishing, 2015: pp. 247–270. https://doi.org/10.1016/B978-0-08-100137-0.00010-9.
- [2] W.R.K. Illeperuma, J.-Y. Sun, Z. Suo, J.J. Vlassak, Fiber-reinforced tough hydrogels, Extreme Mechanics Letters. 1 (2014) 90–96. https://doi.org/10.1016/j.eml.2014.11.001.
- [3] X. Feng, Z. Ma, J.V. MacArthur, C.J. Giuffre, A.F. Bastawros, W. Hong, A highly stretchable double-network composite, Soft Matter. 12 (2016) 8999–9006. https://doi.org/10.1039/C6SM01781A.
- [4] D.R. King, T.L. Sun, Y. Huang, T. Kurokawa, T. Nonoyama, A.J. Crosby, J.P. Gong, Extremely tough composites from fabric reinforced polyampholyte hydrogels, Mater. Horiz. 2 (2015) 584–591. https://doi.org/10.1039/C5MH00127G.
- [5] Y. Huang, D.R. King, T.L. Sun, T. Nonoyama, T. Kurokawa, T. Nakajima, J.P. Gong, Energy-Dissipative Matrices Enable Synergistic Toughening in Fiber Reinforced Soft Composites, Advanced Functional Materials. 27 (2017) 1605350. https://doi.org/10.1002/adfm.201605350.
- [6] Y. Huang, D.R. King, W. Cui, T.L. Sun, H. Guo, T. Kurokawa, H.R. Brown, C.-Y. Hui, J.P. Gong, Superior fracture resistance of fiber reinforced polyampholyte hydrogels achieved by extraordinarily large energy-dissipative process zones, J. Mater. Chem. A. 7 (2019) 13431–13440. https://doi.org/10.1039/C9TA02326G.
- [7] T.L. Sun, T. Kurokawa, S. Kuroda, A.B. Ihsan, T. Akasaki, K. Sato, Md.A. Haque, T. Nakajima, J.P. Gong, Physical hydrogels composed of polyampholytes demonstrate high toughness and viscoelasticity, Nature Mater. 12 (2013) 932–937. https://doi.org/10.1038/nmat3713.
- [8] S. Hong, D. Sycks, H.F. Chan, S. Lin, G.P. Lopez, F. Guilak, K.W. Leong, X. Zhao, 3D Printing: 3D Printing of Highly Stretchable and Tough Hydrogels into Complex, Cellularized Structures (Adv. Mater. 27/2015), Advanced Materials. 27 (2015) 4034–4034. https://doi.org/10.1002/adma.201570182.
- [9] P. Li, Y.F. Poon, W. Li, H.-Y. Zhu, S.H. Yeap, Y. Cao, X. Qi, C. Zhou, M. Lamrani, R.W. Beuerman, E.-T. Kang, Y. Mu, C.M. Li, M.W. Chang, S.S. Jan Leong, M.B. Chan-Park, A polycationic antimicrobial and biocompatible hydrogel with microbe membrane suctioning ability, Nature Mater. 10 (2011) 149–156. https://doi.org/10.1038/nmat2915.
- [10] A. Phadke, C. Zhang, B. Arman, C.-C. Hsu, R.A. Mashelkar, A.K. Lele, M.J. Tauber, G. Arya, S. Varghese, Rapid self-healing hydrogels, Proceedings of the National Academy of Sciences. 109 (2012) 4383–4388. https://doi.org/10.1073/pnas.1201122109.
- [11] M.C. Koetting, J.T. Peters, S.D. Steichen, N.A. Peppas, Stimulus-responsive hydrogels: Theory, modern advances, and applications, Materials Science and Engineering: R: Reports. 93 (2015) 1–49. https://doi.org/10.1016/j.mser.2015.04.001.
- [12] J.P. Gong, T. Kurokawa, T. Narita, G. Kagata, Y. Osada, G. Nishimura, M. Kinjo, Synthesis of Hydrogels with Extremely Low Surface Friction, J. Am. Chem. Soc. 123 (2001) 5582–5583. https://doi.org/10.1021/ja003794q.
- [13] I. Banerjee, R.C. Pangule, R.S. Kane, Antifouling Coatings: Recent Developments in the Design of Surfaces That Prevent Fouling by Proteins, Bacteria, and Marine Organisms, Advanced Materials. 23 (2011) 690–718. https://doi.org/10.1002/adma.201001215.
- [14] J. Shintake, V. Cacucciolo, D. Floreano, H. Shea, Soft Robotic Grippers, Adv. Mater. 30 (2018) 1707035. https://doi.org/10.1002/adma.201707035.

- [15] W.A. Scelzo, S. Backer, M.C. Boyce, Mechanistic Role of Yarn and Fabric Structure in Determining Tear Resistance of Woven Cloth: Part I: Understanding Tongue Tear, Textile Research Journal. 64 (1994) 291–304. https://doi.org/10.1177/004051759406400506.
- [16] E. Triki, T. Vu-Khanh, P. Nguyen-Tri, H. Boukehili, Mechanics and mechanisms of tear resistance of woven fabrics, Theoretical and Applied Fracture Mechanics. 61 (2012) 33–39. https://doi.org/10.1016/j.tafmec.2012.08.004.
- [17] N. Pan, Analysis of woven fabric strengths: Prediction of fabric strength under uniaxial and biaxial extensions, Composites Science and Technology. 56 (1996) 311–327. https://doi.org/10.1016/0266-3538(95)00114-X.
- [18] S.L. Phoenix, I.J. Beyerlein, Statistical Strength Theory for Fibrous Composite Materials, in: Comprehensive Composite Materials, Elsevier, 2000: pp. 559–639. https://doi.org/10.1016/B0-08-042993-9/00056-5.
- [19] Y. Swolfs, I. Verpoest, L. Gorbatikh, A review of input data and modelling assumptions in longitudinal strength models for unidirectional fibre-reinforced composites, Composite Structures. 150 (2016) 153–172. https://doi.org/10.1016/j.compstruct.2016.05.002.
- [20] J.M. Hedgepeth, Stress concentrations in filamentary structures, NASA TN D-882. (1961).
- [21] J.M. Hedgepeth, P. Van Dyke, Local Stress Concentrations in Imperfect Filamentary Composite Materials, Journal of Composite Materials. 1 (1967) 294–309. https://doi.org/10.1177/002199836700100305.
- [22] I.J. Beyerlein, S.L. Phoenix, Stress concentrations around multiple fiber breaks in an elastic matrix with local yielding or debonding using quadratic influence superposition, Journal of the Mechanics and Physics of Solids. 44 (1996) 1997–2039. https://doi.org/10.1016/S0022-5096(96)00068-3.
- [23] D.G. Harlow, S.L. Phoenix, The Chain-of-Bundles Probability Model For the Strength of Fibrous Materials I: Analysis and Conjectures, Journal of Composite Materials. 12 (1978) 195–214. https://doi.org/10.1177/002199837801200207.
- [24] S. Pimenta, S.T. Pinho, Hierarchical scaling law for the strength of composite fibre bundles, Journal of the Mechanics and Physics of Solids. 61 (2013) 1337–1356. https://doi.org/10.1016/j.jmps.2013.02.004.
- [25] M. Ibnabdeljalil, W.A. Curtin, Strength and reliability of fiber-reinforced composites: Localized load-sharing and associated size effects, International Journal of Solids and Structures. 34 (1997) 2649–2668. https://doi.org/10.1016/S0020-7683(96)00179-5.
- [26] H.E. Daniels, The statistical theory of the strength of bundles of threads. I, Proceedings of the Royal Society of London. Series A. Mathematical and Physical Sciences. 183 (1945) 405–435. https://doi.org/10.1098/rspa.1945.0011.
- [27] B.W. Rosen, Tensile failure of fibrous composites, AIAA Journal. 2 (1964) 1985–1991. https://doi.org/10.2514/3.2699.
- [28] W.A. Curtin, Theory of Mechanical Properties of Ceramic-Matrix Composites, J American Ceramic Society. 74 (1991) 2837–2845. https://doi.org/10.1111/j.1151-2916.1991.tb06852.x.
- [29] H.L. Cox, The elasticity and strength of paper and other fibrous materials, British Journal of Applied Physics. 3 (1952) 72–79. https://doi.org/10.1088/0508-3443/3/3/302.
- [30] F. Hikami, T.-W. Chou, Explicit crack problem solutions of unidirectional composites Elastic stress concentrations, AIAA Journal. 28 (1990) 499–505. https://doi.org/10.2514/3.10420.
- [31] C.-Y. Hui, Z. Liu, S.L. Phoenix, Size effect on elastic stress concentrations in unidirectional fiber reinforced soft composites, Extreme Mechanics Letters. 33 (2019) 100573. https://doi.org/10.1016/j.eml.2019.100573.
- [32] I.J. Beyerlein, S.L. Phoenix, A.M. Sastry, Comparison of shear-lag theory and continuum fracture mechanics for modeling fiber and matrix stresses in an elastic cracked composite lamina, International Journal of Solids and Structures. 33 (1996) 2543–2574. https://doi.org/10.1016/0020-7683(95)00172-7.
- [33] Y. Sha, C.Y. Hui, A. Ruina, E.J. Kramer, Continuum and Discrete Modeling of Craze Failure at a Crack Tip in a Glassy Polymer, Macromolecules. 28 (1995) 2450–2459. https://doi.org/10.1021/ma00111a044.
- [34] I.J. Beyerlein, S.L. Phoenix, Statistics for the strength and size effects of microcomposites with four carbon fibers in epoxy resin, Composites Science and Technology. 56 (1996) 75–92. https://doi.org/10.1016/0266-3538(95)00131-X.

- [35] F. Tanaka, T. Okabe, H. Okuda, I.A. Kinloch, R.J. Young, Factors controlling the strength of carbon fibres in tension, Composites Part A: Applied Science and Manufacturing. 57 (2014) 88–94. https://doi.org/10.1016/j.compositesa.2013.11.007.
- [36] W. Weibull, A statistical distribution function of wide applicability, Journal of Applied Mechanics. 18 (1951) 293–297.
- [37] L. Mullins, Softening of Rubber by Deformation, Rubber Chemistry and Technology. 42 (1969) 339–362. https://doi.org/10.5254/1.3539210.
- [38] R.E. Webber, C. Creton, H.R. Brown, J.P. Gong, Large Strain Hysteresis and Mullins Effect of Tough Double-Network Hydrogels, Macromolecules. 40 (2007) 2919–2927. https://doi.org/10.1021/ma062924y.
- [39] Y. Mao, S. Lin, X. Zhao, L. Anand, A large deformation viscoelastic model for double-network hydrogels, Journal of the Mechanics and Physics of Solids. 100 (2017) 103–130. https://doi.org/10.1016/j.jmps.2016.12.011.
- [40] B.D. Coleman, On the strength of classical fibres and fibre bundles, Journal of the Mechanics and Physics of Solids. 7 (1958) 60–70. https://doi.org/10.1016/0022-5096(58)90039-5.
- [41] M. Abramowitz, I.A. Stegun, Handbook of mathematical functions: with formulas, graphs, and mathematical tables, Courier Corporation, 1964.
- [42] Z. Wang, C. Xiang, X. Yao, P. Le Floch, J. Mendez, Z. Suo, Stretchable materials of high toughness and low hysteresis, Proc Natl Acad Sci USA. 116 (2019) 5967–5972. https://doi.org/10.1073/pnas.1821420116.
- [43] J.P. Gong, Y. Katsuyama, T. Kurokawa, Y. Osada, Double-Network Hydrogels with Extremely High Mechanical Strength, Advanced Materials. 15 (2003) 1155–1158. https://doi.org/10.1002/adma.200304907.
- [44] J.P. Gong, Why are double network hydrogels so tough?, Soft Matter. 6 (2010) 2583. https://doi.org/10.1039/b924290b.
- [45] J. Guo, R. Long, K. Mayumi, C.-Y. Hui, Mechanics of a Dual Cross-Link Gel with Dynamic Bonds: Steady State Kinetics and Large Deformation Effects, Macromolecules. 49 (2016) 3497–3507. https://doi.org/10.1021/acs.macromol.6b00421.

Supplementary Information

1. Derivation of (27a,b)

The mean strength $\bar{\sigma}_{\max}(m)$ can be found as

$$\begin{split} & \bar{\sigma}_{\max}\left(m\right) = m \int_{-\infty}^{\infty} \left[1 - G\left(\sigma, l_{T}\right)\right]^{m-1} \frac{dG}{d\sigma} \sigma d\sigma \\ & = \frac{m}{\sqrt{2\pi}\gamma^{*}} \int_{-\infty}^{\infty} \left[1 - \frac{1}{\sqrt{2\pi}} \int_{-\infty}^{(\sigma - \bar{\sigma}_{\max})/\gamma_{n}^{*}} e^{-r^{2}/2} dr\right]^{m-1} e^{-\left[(\sigma - \bar{\sigma}_{\max})/\gamma_{n}^{*}\right]^{2}/2} \sigma d\sigma \\ & = \frac{m}{\sqrt{2\pi}\gamma^{*}} \int_{-\infty}^{\infty} \left[\frac{1}{2} erfc\left[\left(\sigma - \bar{\sigma}_{\max}\right)/\sqrt{2}\gamma_{n}^{*}\right]\right]^{m-1} e^{-\left[\left(\sigma - \bar{\sigma}_{\max}\right)/\sqrt{2}\gamma_{n}^{*}\right]^{2}} \sigma d\sigma \\ & = \frac{m}{\sqrt{\pi}} \left[1/2\right]^{m-1} \int_{-\infty}^{\infty} \left[erfc\left(\eta\right)\right]^{m-1} e^{-\eta^{2}} \left(\sqrt{2}\gamma_{n}^{*}\eta + \bar{\sigma}_{\max}\right) d\eta \end{split}$$
 (S1a)

where we have used

$$\frac{dG}{d\sigma} = \frac{1}{\sqrt{2\pi}\gamma_n^*} e^{-\left((\sigma - \bar{\sigma}_{\max})/\gamma_n^*\right)^2/2}$$
(S1b)

$$1 - \frac{1}{\sqrt{2\pi}} \int_{-\infty}^{(\sigma - \bar{\sigma}_{\max})/\gamma_n^*} e^{-r^2/2} dr = 1 - \underbrace{\frac{1}{\sqrt{2\pi}} \int_{-\infty}^{0} e^{-r^2/2} dr}_{1/2} - \underbrace{\frac{1}{\sqrt{2\pi}} \int_{0}^{(\sigma - \bar{\sigma}_{\max})/\sqrt{2}\gamma_n^*}}_{1/2} e^{-r^2/2} dr$$

$$= \frac{1}{2} - \underbrace{\frac{2}{2\sqrt{\pi}} \int_{0}^{(\sigma - \bar{\sigma}_{\max})/\sqrt{2}\gamma_n^*}}_{0} e^{-\eta^2} d\eta$$

$$= \frac{1}{2} erfc \Big[(\sigma - \bar{\sigma}_{\max})/\sqrt{2}\gamma_n^* \Big]$$
(S1c)

Integration by parts implies that

$$\int_{-\infty}^{\infty} \left[erfc(\eta) \right]^{m-1} e^{-\eta^{2}} d\eta = -\frac{\sqrt{\pi}}{2} \int_{-\infty}^{\infty} \left[erfc(\eta) \right]^{m-1} \frac{derfc(\eta)}{d\eta} d\eta$$

$$= -\frac{\sqrt{\pi}}{2} \frac{\left[erfc(\eta) \right]^{m}}{m} \bigg|_{-\infty}^{\infty} = \frac{\sqrt{\pi}}{2} \frac{2^{m}}{m} \tag{S2}$$

Substituting (S2) into (S1a), $\bar{\sigma}_{max}(m)$ is

$$\bar{\sigma}_{\max}(m) = \bar{\sigma}_{\max} + \frac{m}{\sqrt{\pi}} \sqrt{2} \gamma_n^* \int_{-\infty}^{\infty} \left[erfc(\eta) / 2 \right]^{m-1} e^{-\eta^2} \eta d\eta$$
(S3)

Note, for the chain-of-ELS-bundles model, $\overline{\sigma}_{\max}$ is evaluated at the length $L = l_T$, so that $\overline{\sigma}_{\max} = \overline{\sigma}_{\max} (m = 1)$.

Next, we show
$$I_m = \frac{m}{\sqrt{\pi}} \sqrt{2} \gamma_n^* \int_{-\infty}^{\infty} \left[erfc(\eta)/2 \right]^{m-1} e^{-\eta^2} \eta d\eta < 0$$
 for $m \ge 2$. This is easy since

$$I_{m} = -\frac{m\gamma_{n}^{*}}{\sqrt{2\pi}} \left[\int_{-\infty}^{\infty} \left[erfc(\eta)/2 \right]^{m-1} de^{-\eta^{2}} \right]$$

$$= -\frac{m\gamma_{n}^{*}}{\sqrt{2\pi}} \left[e^{-\eta^{2}} \left[erfc(\eta)/2 \right]^{m-1} \right]_{-\infty}^{\infty} - 2^{-m+1} \int_{-\infty}^{\infty} e^{-\eta^{2}} \frac{d \left[erfc(\eta) \right]^{m-1}}{d\eta} d\eta \right]$$

$$= -\frac{m(m-1)2^{-m+2}\gamma_{n}^{*}}{\sqrt{2\pi}} \left[\int_{-\infty}^{\infty} e^{-2\eta^{2}} \left[erfc(\eta) \right]^{m-2} d\eta \right] < 0$$
(S4)

2. Simulations in sections 3.5 and 3.6

To simulate the stress-strain behavior of one ELS bundle with large N, we first need to generate N random variables, s_j ($1 \le j \le N$), which obey Weibull statistics. We use the random sampling routine, weibull, in the package numpy of Python to draw samples from a Weibull distribution. In section 3.2, we have illustrated a procedure to generate the saw-tooth like stress-strain curve for five fibers. We follow this procedure with N = 1000 fibers. This procedure results in Fig. 7 in the main text with different Weibull shape parameters ρ . We use the following procedure to obtain the stress-strain curves for several chains of ELS bundles. We index a bundle of chain by i ($i = 1, 2, \dots, m$), and denote the stress-strain curve for the i-th bundle by $C^{(i)}$. To illustrate this idea, we use m = 2 and $\rho = 1$ as an example. In Step One, we numerically generate m = 2 stress-strain curves $C^{(i)}$ (i = 1, 2), as indicated by the blue and yellow solid lines in Fig. S1(a). In Step Two, we obtain a stress-strain curve by finding the lower boundary of all $C^{(i)}$, denoted by C and indicated by the black solid line in Fig. S1(b). We repeat the above two steps 1000 times and compute the *mean* of all 1000 curves C; we denote this curve by C^* (red solid line in Fig. S1(c)). In all our simulations, the number of fibers is chosen to be N = 1000.

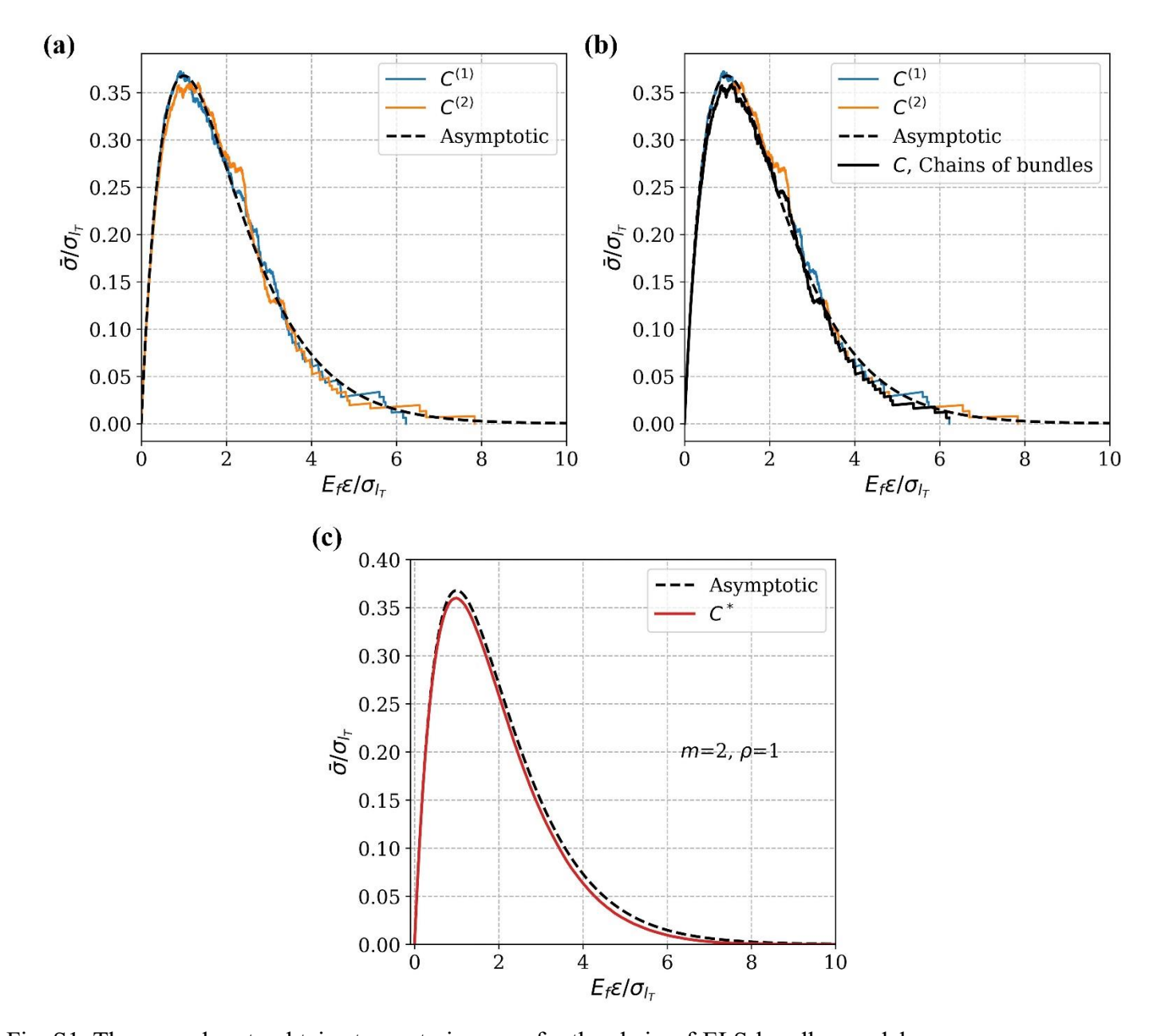


Fig. S1. The procedure to obtain stress-strain curve for the chain-of-ELS-bundles model.

Once we obtain the stress-strain curve C^* , we can use it to compute the mean energy density loss function. In Fig. S2 we plot the stress-strain curve for a several chains of ELS bundles with m=10 and $\rho=1$. The peak value of C^* is denoted by $\bar{\sigma}_{\max}(m)$, and it's asymptotic value for very large N is given by equation (27a,b) in the main text. First, we divide the curve C^* into two regions: the region before the peak value $\bar{\sigma}_{\max}(m)$ is region 1 and the region after, region 2. These two regions are divided by the vertical gray dashed lines in Fig. S2. For Region 1, the curve C^* is found to be approximately equal to the asymptotic solution scaled by $\bar{\sigma}_{\max}(m)/\bar{\sigma}_{\max}(m=1)$, where $\bar{\sigma}_{\max}(m=1)$ is evaluated at the load transfer length l_T in equation (22a) in the main text. For Region 2, the curve C^* is approximately equal to the asymptotic solution (for an equal load sharing bundle, m=1) shifted

downwards by $\overline{\sigma}_{\max}(m=1) - \overline{\sigma}_{\max}(m)$ until it intersects the x-axis. As shown in Fig. S2, this approximation (black dotted line) is in good agreement with C^* . To further verify this approximation, we use different combinations of m and ρ . It demonstrates as long as $m \le 1000$ and $\rho \ge 0.7$, our approximation deviates little from numerical results.

Therefore, in a force-controlled test the mean energy loss density can be well approximated by the area of the curve in region 1, i.e.,

$$W_{loss}^{F}\left(m\right) = \frac{\overline{\sigma}_{max}\left(m\right)}{\overline{\sigma}_{max}\left(m=1\right)}W_{loss}^{F}\left(m=1\right). \tag{S5}$$

For the displacement-controlled test, the mean energy loss density comes from Region 1 and 2. For Region 1, it is identically equal to $W_{loss}^F(m)$, i.e.,

$$W_{loss}^{D,\text{Region 1}}(m) = W_{loss}^{F}(m). \tag{S6}$$

For Region 2, we need to subtract this area by shifting down the asymptotic curve by $\bar{\sigma}_{\max}(m=1) - \bar{\sigma}_{\max}(m)$. The intersection position, η , of our approximation (black dotted line) with the *x*-axis is given by the solution of

$$\overline{\sigma}_{\max}(m) - \overline{\sigma}_{\max}(m=1) = E_f \eta \exp \left| -\left(E_f \eta / \sigma_0\right)^{\rho} \right|, \tag{S7}$$

where the LHS of (S7) is the amount shifted downward, and RHS is the asymptotic solution for one ELS bundle. Also, we notice that the vertical gray line intersects the *x*-axis at the position $\sigma_{l_r} \rho^{-1/\rho} / E_f$. Hence, the contribution from the Region 2 is approximately

$$W_{loss}^{D,\text{Region 2}}\left(m\right) = \left[W_{loss}^{D}\left(m=1\right) - W_{loss}^{F}\left(m=1\right)\right] - \left[\overline{\sigma}_{\text{max}}\left(m=1\right) - \overline{\sigma}_{\text{max}}\left(m\right)\right]\left(\eta - \frac{\sigma_{l_{T}}\rho^{-1/\rho}}{E_{f}}\right)$$
(S8)

where the first term of $W_{loss}^D(m=1) - W_{loss}^F(m=1)$ in RHS corresponds to the area under the asymptotic curve in Region 2, and the second term is the amount we need to subtract due to shift.

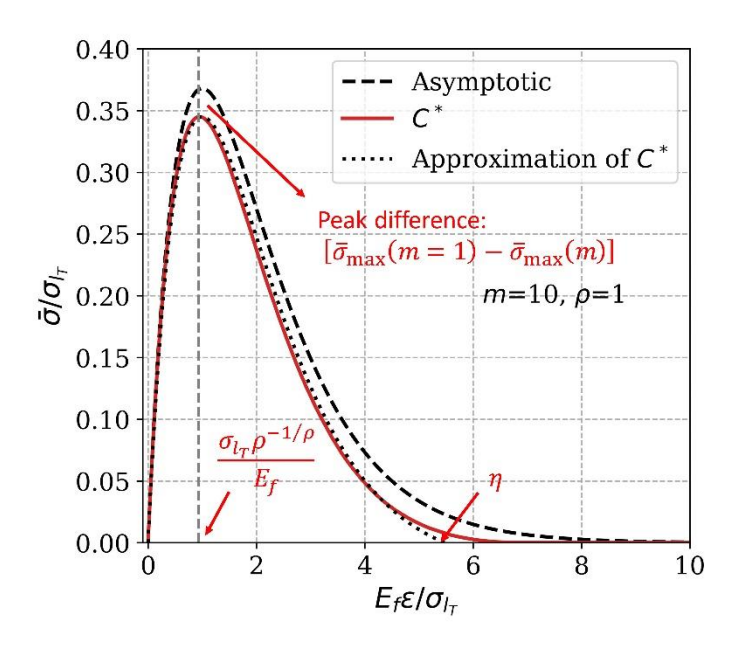


Fig. S2. Stress-strain curve for a chain of ELS bundles with m = 10 and $\rho = 1$.

3. Comparison of equations (34a,b) with finite element solution

To demonstrate the accuracy of our analytical results in Fig. 10, we simulate one case with $\overline{L}_2 = 5$ (normalized height of composite equals to 5 times the load transfer length, see Fig.10(a)) by finite element method (FEM). The finite element model is shown schematically in Fig. S3, and was implemented using the commercial FEM software ABAQUS. The composite, loaded under plane stress conditions, contains 100 square cross-section fibers, and half of these fibers (50 on the left) are broken in the middle to mimic the long pre-crack. Due to symmetry, only the upper half domain is modeled. The ratio of Young's modulus of fiber (E_f) to the shear modulus of matrix (μ_m) is $E_f / \mu_m = 10^4$. The Poisson's ratios of fiber and matrix are 0.3 and 0.49, respectively. The thickness of the square cross-section fiber (h) is equal to the width between adjacent fibers (w). The height of the half composite is $L_2 = 500h$. In such way, the load transfer length is $l_T = 100h$, and $\overline{L}_2 = L_2 / l_T = 5$. On the top edge, a vertical displacement $\Delta = \varepsilon L_2$ is imposed, where ε is the average applied strain. The crack tip is located on the left edge of the first intact fiber. On the bottom edge and behind the crack tip, it is traction free; in front of the crack tip, the vertical displacement and shear traction are prescribed to be zero. To avoid rigid body motion, the horizontal displacement at the crack tip is set to zero. To balance the accuracy and efficiency of the computation, we choose a fine mesh near the crack tip, while far away the element size increases rapidly. Our convergence test shows that further refinement of mesh does not affect the FE results.

We extract the average normal stress $\sigma_{L_2}^{\text{FEM}}$ along the first intact fiber (s=1) and plotted $\varepsilon E_f / \sigma_{L_2}^{\text{FEM}}$ as a function of its vertical coordinate \overline{y} in Fig. S4 (solid line). Our theoretical prediction $\varepsilon C_{22} / \sigma_{L_2}$ where σ_{L_2} is given by (34a) with s=1 is also plotted for comparison. As it shows, our results agree very well with the FEM.

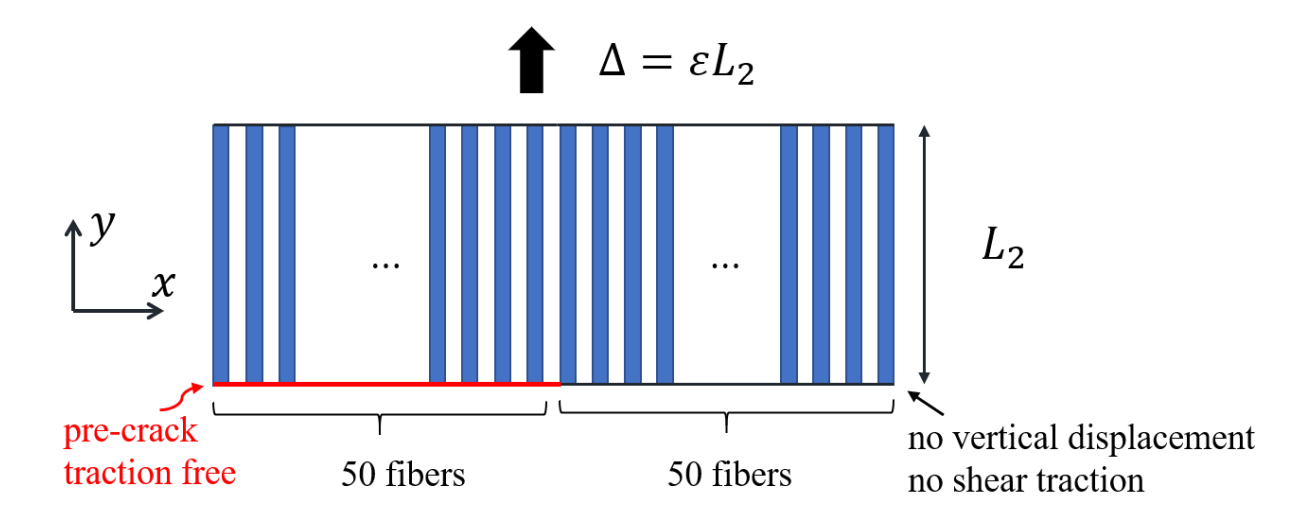


Fig. S3. Schematic of finite element model and boundary conditions. Fibers are highlighted in blue.

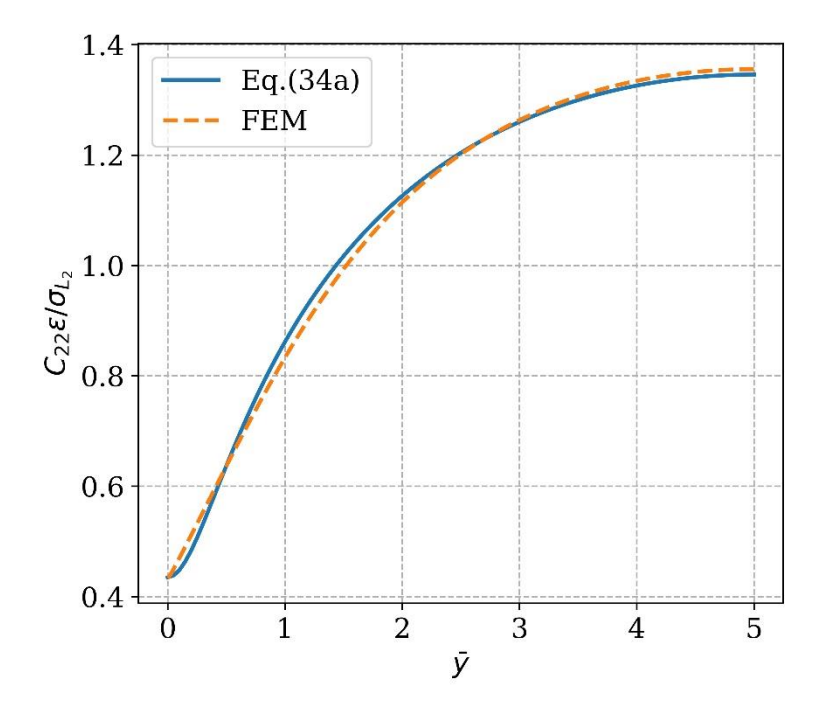


Fig. S4. Comparison of our theoretical results with FEM results along the first intact fiber.